Nanomaterial-Based Plasmon-Enhanced Infrared Spectroscopy

*Xiaoxia Yang, Zhipei Sun, Tony Low, Hai Hu, Xiangdong Guo, F. Javier García de Abajo, Phaedon Avouris, and Qing Dai**

Surface-enhanced infrared absorption (SEIRA) has attracted increasing attention due to the potential of infrared spectroscopy in applications such as molecular trace sensing of solids, polymers, and proteins, specifically fueled by recent substantial developments in infrared plasmonic materials and engineered nanostructures. Here, the significant progress achieved in the past decades is reviewed, along with the current state of the art of SEIRA. In particular, the plasmonic properties of a variety of nanomaterials are discussed (e.g., metals, semiconductors, and graphene) along with their use in the design of efficient SEIRA configurations. To conclude, perspectives on potential applications, including single-molecule detection and in vivo bioassays, are presented.

1. Introduction

Infrared (IR) spectroscopy has played an increasingly important role for material identification through probing the atomic vibrations of a broad range of molecular species and compounds.[1] Specifically, Fourier transform infrared (FTIR) spectroscopy has been widely used for the identification of chemical and biological materials, as it allows rapid, noninvasive, and highly sensitive characterization of molecular fingerprints.[2,3] However, because the wavelength of mid-infrared (mid-IR) light (from 4 to 25 µm) is about three orders of magnitude larger than the typical molecule size (≈10 nm), the cross section of light–molecule interactions becomes remarkably small.[4] This leads to an extremely low sensitivity of IR light for the detection of molecules, which severely limits the range of applications based on trace chemical detection, such as food safety and biosensing.

Surface-enhanced infrared absorption (SEIRA) has been shown to significantly increase the detection sensitivity in the IR up to several orders of magnitude via enhanced light–matter interactions assisted by surface-plasmon polaritons (SPPs).[5–10] SEIRA was first demonstrated with Au and Ag films in 1980.[11] During subsequent decades, most studies remained focused on such a thin-film approach, and in particular, on roughened metal surfaces and films decorated with nanoparticles.[12–15] An advantage of this approach was that it did not require advanced nanofabrication, which was still in its infancy at the time. As a result, there was no significant progress in the engineering of materials with IR plasmonic enhancement.[12–15] However, recent advances in nanofabrication technologies have enabled the preparation of well-defined metallic nanostructures exhibiting IR plasmonic enhancement much larger than the previously observed in thin-film structures.[9,10] Subsequently, numerous SEIRA nanoscale morphologies[5,16–18] have been proposed and experimentally demonstrated to significantly enhance the resonance signals for an expanding range of applications.[7,8,19,20]

Most recently, renewed interest in new IR plasmonic materials (e.g., graphene,[21–26] Si,[27] Ge,[28–31] InAs,[32,33] InSb,[34] InAsSb,[35] oxides,[36,37] and carbon nanotubes (CNTs)[38,39]) has arisen within the community, extensively pushing the development of SEIRA.[40,41] Among these materials, graphene has been a central focus of attention because of its unique plasmonic properties. Specifically, it features mid-IR plasmons, supported by two-dimensional (2D) Dirac fermion electronic states,[42] which can produce extremely high field confinement with low damping (up to ≈1 ps lifetime[43]), reaching plasmon wavelengths two orders of magnitude smaller than the free-space light wavelength for attainable doping densities[22,24,26,44] (i.e., ≈20-fold improvement over plasmons in typical Au antennas[45]). Additionally, graphene plasmons can be tuned in

Prof. X. Yang, H. Hu, X. Guo, Prof. Q. Dai
Division of Nanophotonics
CAS Center for Excellence in Nanoscience
National Center for Nanoscience and Technology
Beijing 100190, China
E-mail: daiq@nanoctr.cn
Prof. X. Yang, H. Hu, X. Guo, Prof. Q. Dai
University of Chinese Academy of Sciences
Beijing 100049, P. R. China
Prof. Z. Sun
Department of Electronics and Nanoengineering
Aalto University
Tietotie 3, FI-02150 Espoo, Finland
Prof. Z. Sun
QTF Centre of Excellence
Department of Applied Physics
Aalto University
FI-00076 Aalto, Finland
Prof. T. Low
Department of Electrical and Computer Engineering
University of Minnesota
Keller Hall 200 Union St S.E., Minneapolis, MN 55455, USA
Prof. F. J. García de Abajo
ICFO-The Institute of Photonic Sciences
The Barcelona Institute of Science and Technology
08860 Barcelona, Spain
Prof. F. J. García de Abajo
ICREA-Institució Catalana de Recerca I Estudis Avançats
Passeig Lluís Companys 23, 08010 Barcelona, Spain
Prof. P. Avouris
IBM T. J. Watson Research Center
Yorktown Heights, NY 10598, USA

DOI: 10.1002/adma.201704896

frequency by varying the doping level, for example using electrical gates.[25,26] Active tunability is a long-awaited property in plasmonics, which positively impacts SEIRA by enabling highly selective detection of multiband molecular vibrational modes over a wide IR range. Because of all of these unique properties, graphene plasmons have emerged as an outstanding SEIRA platform over the past two years.[4,46–50]

Here, we discuss recent progress in the development of SEIRA, its applications, and some future perspectives. We first present in Section 2 a tutorial overview of the physical principles of IR plasmonic enhancement, followed in Section 3 by a survey of SEIRA phenomena in various material platforms, including traditional metals, semiconducting nanomaterials, and graphene. We devote Section 4 to discussing future trends and potential applications of SEIRA. Finally, we conclude with a brief outlook in Section 5.

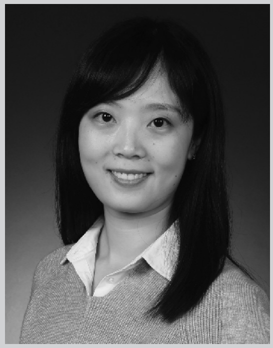

Xiaoxia Yang is an Associate Professor of the National Center of Nanoscience and Technology, China. She received her B.Sc. in materials and M.Sc. in microelectronics from Wuhan University in 2007 and 2009, and Ph.D. in physics from Institute of Physics, Chinese Academy of Sciences in 2012. Her main research interests are 2D materials and nanophotonics.

Qing Dai is a Professor of the National Center of Nanoscience and Technology, China. He received his M.Eng. in electronic and electrical engineering from Imperial College, London, in 2007 and Ph.D. in nanophotonics from the Department of Engineering, University of Cambridge in 2011. His main research interests are low-dimensional materials, optoelectronics, and nanophotonics.

2. Fundamentals of SEIRA

2.1. IR Plasmonics

SEIRA relies on high-quality, high-wave-vector, and tunable plasmon excitations—collective oscillations of free charge carriers in conducting materials—in the IR range. The former two properties are responsible for a strong field enhancement that ultimately increases the level of optical absorption by molecules placed inside the plasmonic hotspots. Remarkably, plasmons can be predictively described through a classical level of theory relying on the solution of Maxwell's equations for the morphologies under consideration, using the bulk, frequency-dependent permittivities of the materials involved to capture their optical response. In particular, the free-carrier-driven response of metals,[45,51] semiconductors,[28] and graphene[22] in the IR frequency range can be accurately described by the Drude model, which predicts a complex permittivity[52]

$$\varepsilon(\omega) = \varepsilon' + \mathrm{i}\varepsilon'' = \varepsilon_\infty - \frac{\omega_\mathrm{p}^2}{\omega^2 + \mathrm{i}\gamma\omega} = \varepsilon_\infty - \frac{\omega_\mathrm{p}^2}{\left(\omega^2 + \gamma^2\right)} + \mathrm{i}\frac{\omega_\mathrm{p}^2\gamma}{\left(\omega^2 + \gamma^2\right)\omega} \quad (1)$$

$$\omega_\mathrm{p}\left(\mathrm{cm}^{-1}\right) = \frac{1}{2\pi c}\left(\frac{4\pi^2 ne^2}{m^*\ \varepsilon_\infty}\right)^{1/2} \quad (2)$$

$$\gamma\left(\mathrm{cm}^{-1}\right) = \frac{e}{2\pi c\mu\ m^*} \quad (3)$$

Here, ω is the optical frequency, ε' and ε'' are the real and imaginary parts of $\varepsilon(\omega)$, ε_∞ is the high-frequency dielectric constant, ω_p is the classical plasma frequency, γ is the Drude relaxation rate, c is the speed of light in vacuum, n is the volume density of free carriers, e is the electron charge, m^* is the effective mass of those carriers, and μ is the carrier mobility. The relaxation time can be conveniently expressed in terms of the carrier lifetime τ as $\gamma\ (\mathrm{cm}^{-1}) = \frac{1}{2\pi c\tau}$. Note that we introduce a factor $\frac{1}{2\pi c}$ in Equations (2) and (3), so that all frequencies are expressed in units of cm^{-1}, which are customary in IR spectroscopic notation. Equations (1) and (2) describe three-dimensional (3D) materials with parabolic electron dispersion, leading to a scaling $\omega_\mathrm{p} \propto \left(\frac{n}{m^*}\right)^{1/2}$, while a different relationship is obtained for materials with a nonparabolic dispersion or when they are 2D or one-dimensional (1D).[53] In particular, for massless Dirac fermion plasma, in which the electronic dispersion is conical, one has $\omega_\mathrm{p} \propto n^{1/3}v_\mathrm{F}^{1/2}$, $n^{1/4}v_\mathrm{F}^{1/2}$, and $n^0 v_\mathrm{F}^{1/2}$ in 3D, 2D, and 1D, respectively, where v_F is the Fermi velocity (i.e., the slope of the conical electronic band).[53]

As a general rule, the existence of plasmons requires that the permittivity ε has a negative real part ($\varepsilon' < 0$). Plasmons are then sustained at the interface with a medium of positive permittivity (e.g., a dielectric such as glass, air, or water). According to Equation (1), the condition $\varepsilon' < 0$ is satisfied if the plasma frequency of the material is higher than the targeted IR frequency. Combined with Equation (2), we can estimate that the required free-carrier concentration n should be roughly $>10^{19}\ \mathrm{cm}^{-3}$ for materials with parabolic electron dispersion and $m^* \approx m_\mathrm{e}$. For thin films, this translates into charge-carrier densities $>10^{12}\ \mathrm{cm}^{-2}$ per nm of thickness. Measured spectral curves of ε' and ε'' are plotted in **Figure 1** for representative metals (Au, Ag, Cu, and Al),[54] semiconductors (silicide,[55] doped Si,[27] Ge,[56] InSb[34] and InAs[33]), and graphene.[24] Note that metals typically host about one or more free electrons per atom, whereas the carrier concentrations of semiconductors and graphene are two orders of magnitude smaller. This implies significantly higher plasma frequency in metals, or equivalently,

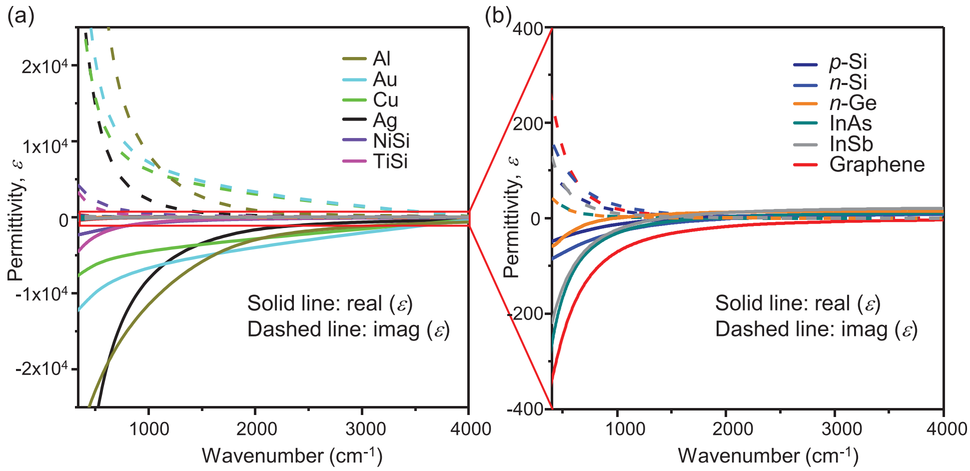

Figure 1. a) Permittivity of representative metals (Au, Ag, Cu, and Al), semiconductors (NiSi with $\omega_p = 0.32$ µm, TiSi with $\omega_p = 0.39$ µm, p-doped Si with $\omega_p = 5.75$ µm, n-doped Si with $\omega_p = 4.47$ µm, and InAs with $\omega_p = 5.5$ µm) and graphene in the Drude model within the relevant IR frequency range of 350–4000 cm^{-1}. b) Enlarged view of the curves in the red rectangle of (a), showing the permittivity of doped Si, n-Ge, InAs, InSb, and graphene. The real and imaginary parts are shown as solid and dashed curves, respectively. Drude model parameters of metals from ref. [54], NiSi and TiSi from ref. [55], doped Si from ref. [27], doped Ge from ref. [56], InAs from ref. [33], InSb from ref. [34]. The graphene permittivity is calculated following ref. [24] with a Fermi energy of 0.2 eV.

more dispersive SPPs. Hence, for a given frequency ω, SPPs in metals have an appreciably smaller wave vector, implying poorer light confinement. Indeed, quantitative comparisons between graphene and silver suggest that light confinement in graphene is about two orders of magnitude stronger in the IR regime.[22,57] Incidentally, we ignore interband processes because they typically involve higher frequencies than those considered within the IR spectral range (except for graphene, in which the condition for the absence of interband transitions is that the Fermi energy roughly exceeds the plasmon energy[58]). An apparently unintuitive result is that plasmon damping occurs at a rate γ independent of both the shape of the structure and the carrier density under the assumptions of the Drude model (Equations (1)–(3)) and the neglect of retardation. This is a direct consequence of the fact that the frequency dependence in the Drude model enters through $\omega + i\gamma$; then, a plasmon mode is signaled by a specific value of the permittivity ε_p, so that the condition $\varepsilon(\omega) = \varepsilon_p$ leads to a complex eigenfrequency with an imaginary part $\approx\gamma/2$, therefore encompassing a time dependence of the intensity given by $e^{-\gamma t}$.

All of the materials considered in Figure 1 possess a negative ε' (solid curves), and thus can support plasmons in the IR. As expected, large $|\varepsilon'|$ values are observed in materials with high carrier density n (e.g., metals), and consequently also large ω_p, while low $|\varepsilon'|$ values are found in semiconductors (i.e., materials with low carrier density and relatively low ω_p). Interestingly, graphene features large values of $|\varepsilon'|$ despite the low doping density n that is attainable through currently available gating technology. This is a result of the conical electronic dispersion, which leads to the scaling $\omega_p \propto n^{1/4}$, in contrast to parabolic materials, for which $\omega_p \propto n^{1/2}$.

The carrier mobility μ and the bulk plasma frequency ω_p are important parameters because they determine the IR absorption, as well a non-radiative (Equation (3)) and radiative damping (see below).[59] They are plotted in **Figure 2** for various representative materials, including metals,[60–62] superconductors,[63,64] graphene,[65–68] topological insulators,[69,70] and

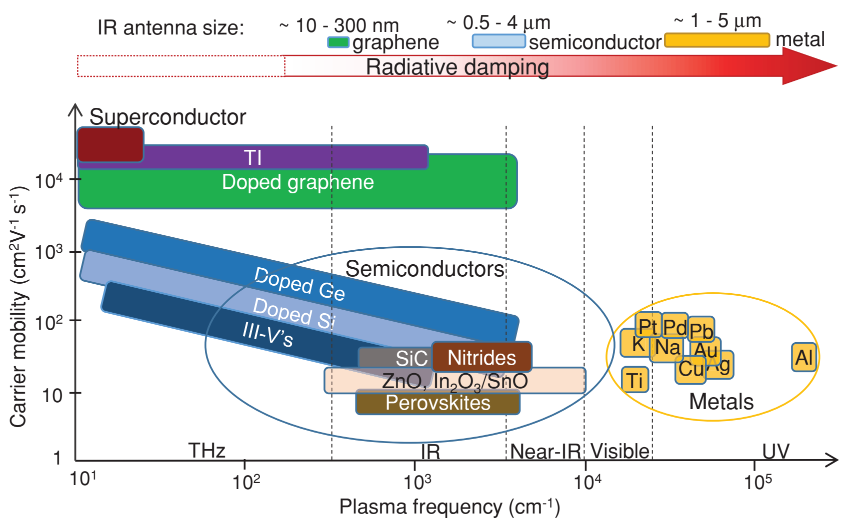

Figure 2. Typical plasmonic materials and their corresponding plasmonic responses. The plasmon damping largely depends on the plasma frequency and carrier mobility. TI: topological insulator. We present parameters for metals (Au, Ag, Al, K, Na;[60] Au, Ag, Cu, Na, Al;[61] Pt, Pb, Pd, and Ti[62]), a superconductor ($YBa_2Cu_3O_{7-d}$),[63,64] graphene,[65,66] two TIs (HgTe[69] and Bi_2Se_3[70]), and various semiconductors (In_2O_3/SnO,[71] ZnO,[71,72] Ge,[28,73] Si,[27,74] III–V's,[75,76] and SiC[77]). The relationship between the size of a dipole plasmon antenna made of these materials and radiative damping is schematically plotted in the upper part. Typical antenna sizes of graphene,[4,46,67,68] semiconductor,[56,78] and metals[17] are indicated.

various semiconductors.[71–78] In general, the existence of IR plasmons requires that ω_p exceeds the optical frequency. However, if ω_p is too high ($>>\omega$), the permittivity takes large values, so that the plasmon wavelength λ_p approaches the light wavelength λ_0, thus incrementing the coupling to propagating light and the effect of radiative damping. This is clearly the case of dipole antennas, which have a characteristic size $\approx\lambda_p/2$. Typical sizes of dipolar antennas made of graphene, semiconductors, and metals are also plotted in Figure 2. The radiative damping of these antennas increases with their size.[79] For instance, the length of an IR dipolar gold antenna is a fraction of the free-space wavelength[9] (the exact value depends on the geometrical aspect ratio[45]), and the plasmon width is typically dominated by radiative losses.[80,81] By virtue of reciprocity, the positive side of this is that a strong coupling to far-field radiation implies a more efficient excitation.

For semiconductor and graphene nanoantennas, the dimensions are much smaller than their resonant free-space wavelength, so their radiative losses are negligible. Nonetheless, intrinsic Ohmic losses cannot be disregarded in semiconductors. A high carrier mobility typically translates into low Ohmic losses. Hence, the ideal materials for SEIRA are those with high mobility μ and featuring an ω_p in the IR region. In semiconductors, ω_p can be tuned to the IR range by doping, but most of these materials have relatively low mobilities at high dopant concentrations.[73,82] In graphene, Ohmic losses can also be very low, particularly in exfoliated samples encapsulated in hexagonal boron nitride (hBN), which have ultrahigh mobilities.[43] Additionally, the electrical tunability of the carrier density in graphene is useful to tune its plasmonic resonances—a property that facilitates applications in selectivity sensing,[4] although the fabrication of high-quality graphene samples still relies on intensive, nonscalable processes.

2.2. Operation Principle of SEIRA: The Coupled Harmonic Oscillator Model

SEIRA shares some similarities with surface-enhanced Raman scattering (SERS). In SEIRA, photons are inelastically absorbed with a probability proportional to the incident light intensity (i.e., the number of incident photons) times the enhancement at the plasmonic hotspot in which the absorbing molecule is placed; in a Stokes (anti-Stokes) SERS process, we first have inelastic absorption like in SEIRA, followed by inelastic reemission at a lower (larger) frequency with a probability also proportional to the intensity enhancement. Additionally, the so-called chemical enhancement can affect the dipole strength of the analyte due to electronic hybridization with (and charge transfer to) the substrate; because of the doubly inelastic character of SERS, chemical enhancement then plays a more important role than in the singly inelastic SEIRA.[3] We refer the reader to the excellent available reviews on the theoretical description of electromagnetic enhancement of SEIRA,[5,17] and only briefly describe it in this section.

In a simplified picture, plasmon coupling to infrared-active atomic vibrational modes in a molecule can be understood in terms of classical coupled harmonic oscillators.[83] We first consider a driven damped harmonic oscillator in one dimension to represent the plasmon, as illustrated in **Figure 3**a. The position x_1 of the effective moving particle follows the equation of motion

$$m_1\ddot{x}_1 + \frac{m_1\dot{x}_1}{\tau_1/2} + k_1\,x_1 = F\cos(\omega t) \tag{4}$$

where m_1 is the mass of the particle, τ_1 is the resonance lifetime, k_1 is the spring constant, and F is the driving force. The latter

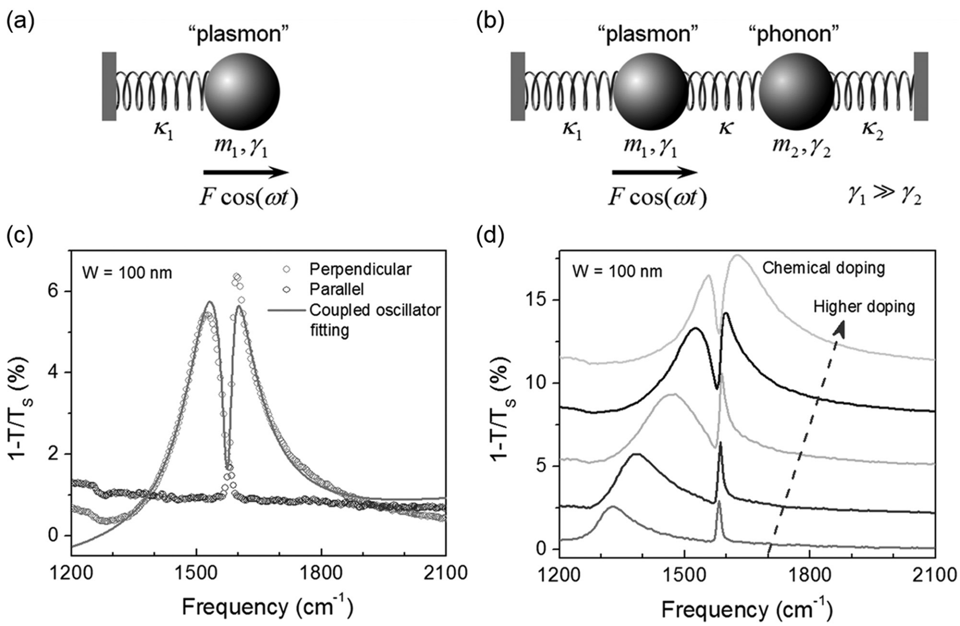

Figure 3. Harmonic-oscillator model for SEIRA. Illustration of: a) a simple damped oscillator and b) two coupled oscillators. c) Extinction spectra obtained from a bilayer graphene nanoribbon array (circles) and the fitting to a coupled oscillator model (curve, see the main text).[85] The ribbon width is $W = 100$ nm. d) Evolution of the extinction spectra with increasing doping.[85] c,d) Reproduced with permission.[85] Copyright 2014, American Chemical Society.

is provided by the incident light of frequency ω. Equation (4) has the solution $x_1(t) = a_1 \cos(\omega t + \varphi_1)$, where

$$a_1 = -\frac{F}{m_1}\frac{1}{\sqrt{\left(\omega^2-\omega_1^2\right)^2+\left(\omega\,\delta\omega_1\right)^2}} \tag{5}$$

is the oscillation amplitude

$$\varphi_1 = \tan^{-1}\left(\frac{\delta\omega_1}{\omega^2-\omega_1^2}\right) \tag{6}$$

is the oscillation phase relative to the incident light, $\omega_1 = \sqrt{k_1/m_1}$ is the resonance frequency and $\delta\omega_1 = 2/\tau_1$ is the damping rate, which also gives the frequency full width at half maximum of the amplitude spectrum. The presence of damping places the maximum of a_1 at a frequency $\omega_{\max} = \sqrt{(\omega_1^2 - \delta\omega_{1/2}^2)} \approx \omega_1$, with the rightmost approximation applicable in the $\omega_1 \gg \delta\omega_1$ limit.

Figure 3b illustrates the coupling between two harmonic oscillators: the driven oscillator 1, representing the plasmon, and oscillator 2, mimicking a molecular vibration. For a coupling rate k between the two oscillators, the equations of motion are as follows [84,85]

$$\begin{aligned} m_1\ddot{x}_1 + \frac{m_1\dot{x}_1}{\tau_1/2} + k_1x_1 - kx_2 &= F\cos(\omega t),\\ m_2\ddot{x}_2 + \frac{m_2\dot{x}_2}{\tau_2/2} + k_2x_2 - kx_1 &= 0 \end{aligned} \tag{7}$$

Because we are interested in the average power absorbed by oscillator 1, we seek a solution for a_1

$$a_1 = -\frac{F\left(\alpha_2^2+\beta_2^2\right)}{\sqrt{\left(k^2\alpha_2-\alpha_1\alpha_2^2-\alpha_1\beta_2^2\right)^2+\left(k^2\beta_2-\beta_1\alpha_2^2-\beta_1\beta_2^2\right)^2}} \tag{8}$$

where $\alpha_j = m_j\,(\omega_j^2 - \omega^2 + k/m_j)$ and $\beta_j = m_j\,\omega\delta\omega_j$. A similar expression for a_2 is also obtained. Finally, we find for the power $P_S(\omega_S)$ absorbed during one period of oscillation of the probe force the expression $P_S(\omega_S) = \omega_S\, a_1 F[1 - \cos(4\pi\omega_S)]$. As an example of application of this simple formalism, we explore next its ability to describe a real situation.

Figure 3c shows typical measured extinction spectra of an AB-stacked bilayer graphene ribbon array for two incident light polarizations, either parallel or perpendicular to the ribbons.[85] The optical response of bilayer graphene in the chosen example has several interesting IR features, including mid-IR plasmons (for perpendicular polarization), the C–C stretching optical phonon at 0.2 eV (for parallel polarization), and the onset of interband absorption at ≈0.4 eV.[86] The plasmon resonance is tuned to coincide with that of the optical phonon. When coupled in the same system, the largely mismatched lifetimes of the plasmon and the phonon results in the emergence of induced transparency, which can be reproduced by the simple coupled oscillator model outlined above. As the plasmon and phonon detuning increases, the induced transparency evolves into a Fano-like structure in the spectra as shown in Figure 3d.

This type of plasmon–phonon coupling can also be understood as a Fano resonance phenomenon, that is, as the coupling between a continuum of modes and a discrete excitation.[9,87] In our case, the continuum is provided by the plasmon, which undergoes strong coupling to light (i.e., it acts as a bright mode) and exhibits a large width, therefore appearing as a quasicontinuum from the point of view of the phonon. In contrast, the phonon does not couple or only couples poorly to light, its spectral width is small, and therefore behaves as a dark discrete mode. This leads to well-known lineshapes as predicted by Fano,[88] characterized by dips as those observed in Figure 3d, essentially due to the destructive interference between the bright and dark modes. The depth of the dip decreases as the detuning increases, and for a completely detuned configuration, the asymmetric vibrational contrast almost disappears.[9] Thus, a minimal detuning nearly in resonance between the plasmon and the molecular vibrational mode is important for obtaining significant enhancement and maximum contrast of the molecular vibrational signal in the absorption spectrum. Among other factors, the interaction strength also depends strongly on the volume density of molecular dipoles, the molecular relaxation time, and the molecular layer thickness.[89]

3. The Current State of the Art of SEIRA

Research on SEIRA has attracted strong interest, and this has translated into enormous advances over the past few decades. In this section, we present the state of the art of SEIRA based on various materials, including metals, semiconductors, graphene, and others.

3.1. Metal-Based SEIRA

The principles of SEIRA were first demonstrated using Au and Ag thin films in the 1980s.[11] Subsequently, SEIRA was widely studied with various nanoisland films[12] and roughened metal surfaces based on both noble metals and transition metals such as Ag, Au, Cu, Pt, Pd, Rh, and Ru.[11,13,14,90,91] **Figure 4**a illustrates a typical atomic-force-microscopy (AFM) image of a SEIRA-active Au film evaporated on an Si substrate, consisting of nanoparticles with an average diameter of ≈70 nm.[14] The plasmonic resonance frequencies of nanoscale metal particles lie in the visible range,[11,12,14,90,92,93] and their mechanism for the SEIRA effect is briefly discussed as follows. The nanoparticles can be polarized by the incident IR light and the induced dipole p generates an enhanced local electric field around the particles (estimated to be about 10 times larger than the incident field), which excites adsorbed molecules (the analytes), as shown in Figure 4b.[3,94] The molecular vibration induces an additional dipole δp in the metal particles and perturbs the effective optical properties of the rough metal film. As a result of this, the molecular vibrations can be observed through the change in absorption or reflectance of the metal film, which further improves the molecules' vibrational signals. Typical IR signal enhancement factors are within a range of 10–100 when based on rough metal films.[11,12,14,90,95] Taking advantage of both the chemical reaction and the field enhancement at the surface of metal electrodes, metal-film-based SEIRA

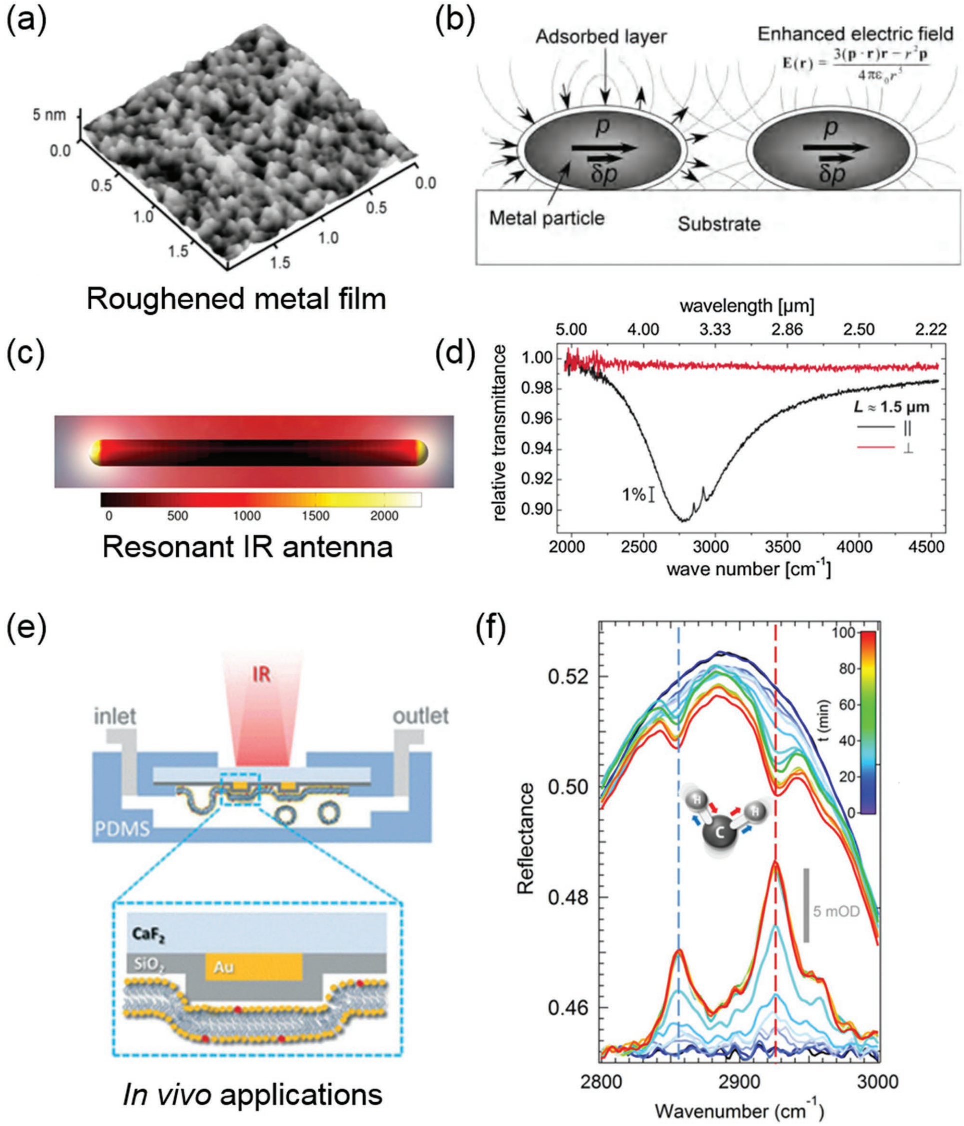

Figure 4. SEIRA based on metal plasmons. a) Roughen metal films.[14] b) Electromagnetic mechanism of metal nanoparticles.[3] A dipole p in each metal nanoparticle driven by incident light excites molecular vibrations, resulting in a dipole change δp. c) IR optical antenna.[9] We show the calculated near-field intensity 1 nm above the surface of a gold nanowire (in vacuum, length $L = 1.31$ µm, diameter 100 nm) at a resonance wavelength 3.41 µm. d) Transmittance spectra of molecules with (black curve) and without (red curve) an Au-antenna-based plasmon resonance.[9] e) Sealed Au antennas for in vivo applications of SEIRA in aqueous solution.[19] f) Real-time SEIRA signal of lipid bilayers formed on Au antennas.[19] a) Reproduced with permission.[14] Copyright 2002, Elsevier. c,d) Reproduced with permission.[9] Copyright 2008, American Physical Society. e,f) Reproduced with permission.[19] Copyright 2016, American Chemical Society.

has been widely used to monitor electrochemical reactions at the electrode/solution interface.[3] In combination with the attenuated total reflection (ATR) configuration, one can further improve the enhancement and largely suppress noisy signals from the sampled solution at the same time.[3,96]

Along with the progress in nanofabrication technologies, highly reproducible structures have been developed. For example, Wang and co-workers[97,98] report the design of patterned arrays of near-infrared (near-IR) resonant gold nanoshells with interparticle gaps of less than 10 nm. In these closely packed arrays, the dipolar plasmons of the individual nanoshells, appearing as narrow visible or near-IR bands, strongly intermix to form hybridized broadband IR (≈2–8 µm) plasmons. The localized field enhancement, which is typically defined by the ratio of the amplitudes associated with the local electric field and the input light electric field (i.e., $|E/E_0|$), is calculated to be ≈30 over a broad mid-IR range at the particle gaps.[97,98] This corresponds to a factor ≈900 in intensity $\propto E^2$, which directly translates into the enhancement factor of the molecular IR signal. Metal films with microarrays of subwavelength holes have also been demonstrated to excite propagating SPPs for SEIRA spectroscopy applications.[99]

Suitably designed IR dipole-antenna structures with prominent resonance peaks at target molecular vibrational frequencies have been fabricated and then widely explored for SEIRA applications since 2008.[9,45,100–102] For example, Neubrech et al.[9] report the fabrication of IR plasmonic antennas based on micrometer-long gold nanowires via electrochemical deposition in etched ion-track membranes, which produced largely enhanced near fields ($|E/E_0| \approx 2000$ in Figure 4c) and a prominent plasmonic resonance absorption peak (Figure 4d). The near-field distribution around gold nanowires has been experimentally measured in detail and is consistent with finite-element simulations.[51,103] The antenna concept was extended into the optical and IR wavelength ranges by adapting concepts borrowed from traditional radio-frequency antenna designs, with slight modifications needed to depart from the perfect-conductor approximation.[45,100] For a half-wave dipole antenna, the resonance wavelength λ is typically given by $\lambda = \frac{2L}{m} na_1 + a_2$, where L is the antenna length, m is the mode number, and n is the refractive index of the surrounding medium.[17,45,104] The constant a_2 accounts for the phase associated with plasmon reflection at the antenna end, while the parameter a_1 depends on the antenna geometry and composition.[17,45,104] According to this simple law, the resonant frequencies can easily be engineered by choosing suitable antenna lengths. For example, when a proper antenna length ($L = 1.5$ µm) is selected, the antenna frequency can be tuned to match well with the molecular vibrational modes.[9] This leads to strong antiresonance features that appear exactly at the molecular vibrational frequencies (2916–2936 and 2850–2863 cm^{-1} of the octadecanthiol molecules[9]) in the plasmonic extinction spectrum, as shown in Figure 4d. This enables the development of resonant SEIRA with unprecedented signal enhancement of up to five orders of magnitude for high sensitivity detection down to the attomolar level.[9] When the length of the antennas is increased or decreased, the plasmonic resonance frequency is respectively red- or blueshifted with respect to the vibrational modes, changing the phase interaction (i.e., modifying the coupling strength in terms of the Fano resonance model) and thus reducing the strength of the measured vibrational signals with clearly asymmetric spectral profiles.[9]

The role of plasmonic absorption and scattering of the hosting antennas has also been studied, while an optimal SEIRA signal measured in transmittance was found to be achieved when the spectral maxima of absorption and scattering of the antennas are of similar magnitude[105] (the so-called critical-coupling condition). The size of IR metal antennas is typically large (>1 µm). Such large structures exhibit significant radiative losses, as discussed in Section 2.2. In the IR regime, these losses constitute the main source of plasmon damping and can largely reduce the plasmon intensity, and subsequently, the enhancement of SEIRA.[80,106] Efforts have been made to mitigate these radiation losses by optimizing the antenna parameters, such as its geometry and dielectric environment.[5,107] Additionally, multiple antennas can be well arranged to achieve destructive interference of radiative losses,[10,108] while spectral narrowing and strength enhancement of the far-field response were demonstrated.[10] More importantly, calculations indicate that the near-field intensities of antenna arrays can be realistically enhanced by a factor of 10^2–10^3 compared to those of individual antennas,[10] essentially relying on the well-known effect of optical phase accumulation produced by periodic-lattice resonances.[109] In experiments, tenfold signal enhancement has been demonstrated in detecting monolayer protein IR spectra based on nanoantenna arrays (yielding an absolute molecular absorption of ≈6.8%) compared with randomized antennas (≈0.9% absorption).[10] Other geometries have also been used to increase the near-field intensity of plasmons,[110] such as antennas with nanometer-sized gaps and antennas supported by metal films.[102,111–114] In Brown et al.,[115] a crossed-field antenna structure was designed in order to form a small gap at the center, resulting in an intensity absorption that increased linearly with the number of antennas in the patterned array. This led to a predicted SEIRA enhancement factor of up to four orders of magnitude. Based on various metallic nanoantenna structures, highly sensitive detection with SEIRA has been demonstrated. For example, in Cubukcu et al.[111] a surface-enhanced molecular detection technique with zeptomole level sensitivity (zepto = 10^{-21}) was created by relying on the resonant coupling of plasmonic modes of split-ring resonators, in which large near-field enhancements were present at the gap. A detailed review of various nanoantenna structures for SEIRA can be found in Neubrech et al.[17] and Biagioni et al.[116]

Besides the efforts aimed at achieving large signal enhancement as mentioned above, research activities oriented toward enriching functionalities of SEIRA have also been pursued.[8,112,114,117,118] For example, simultaneously monitoring the multiple spectral fingerprints of different moieties with SEIRA is of great importance for various applications, as it allows accurate identification of molecular species due to its capability of detecting a large set of IR vibrational modes. In particular, in Wu et al.,[8] an IR plasmonic surface with two resonant peaks constructed from a Fano resonance in an asymmetric metamaterial was introduced, which results from the interference between subradiant and superradiant modes. Such a multipeak resonance can offer signal enhancement for fingerprinting multiple vibrational modes. For instance, the frequency of the subradiant resonance can be precisely adjusted to match the molecule's vibrational fingerprints (e.g., the amide I and II of proteins) for high signal enhancement.[8] Also, Chen et al.[112] describes a dual-band perfect absorber based on an asymmetric gold nanocross structure for the simultaneous detection of two molecular vibrational modes of a 4 nm thick poly(methyl methacrylate) (PMMA) layer. The ability to tune plasmonic resonances via changing the structural geometry, and in particular the in situ dynamic strain, can provide SEIRA with a wide operation bandwidth.[117] Additionally, multifunction of both SEIRA and SERS can be realized based on well-designed metallic nanostructures.[98,119,120] For example, engineered visible and IR plasmons can be selectively excited by incident light with polarization perpendicular and parallel to nanoantennas, respectively.[98,119]

There is great interest in achieving in vivo/in situ characterization of biomolecules or chemical reactions in aqueous solution. Various metallic structures have been demonstrated to realize SEIRA of biomolecules in aqueous solution.[7,19] For example, in Limaj et al.,[19] an IR plasmonic biosensor is described based on gold antennas fabricated on a CaF_2 substrate and sealed in a poly(dimethylsiloxane) (PDMS) fluidic chamber, as shown in Figure 4e. Lipid vesicles were injected in situ, and subsequently ruptured to form lipid bilayers on the supporting antennas for real-time monitoring. The enhanced IR signal of molecules was recorded via reflectance spectra. By exploiting the plasmonic field enhancement in the vicinity of engineered surface-modified gold nanoantennas, a biosensor could detect the vibrational fingerprints of lipid molecules absorbed on the gold nanoantenna surfaces (Figure 4f). The formation kinetics of planar biomimetic membranes in aqueous environments can be monitored in real time. For example, in Adato and Altug,[7] gold nanoantennas were assembled in a fluidic chamber. This approach leveraged the plasmonic enhancement of absorption bands in conjunction with a nonclassical form of internal reflection and enabled in situ monitoring of protein and nanoparticle interactions with high sensitivity in real time. Specifically, minute volumes of water displacement during binding events can be observed by this approach.[7] Information on the conformation of a protein is closely related to its physiological function, and, in this respect, a recent study[121] has demonstrated the secondary structure identification of nanometer-thin proteins in aqueous solution by resolving the content of plasmonically enhanced amide-I signatures.

Among all the metallic materials, gold is the most widely used to fabricate optical antennas because of its stability and biocompatibility. Gold-antenna-based SEIRA structures are compatible with both transmittance- and reflection-measurement configurations, so they can be used for detection in solids, gases, and liquids. Despite these advantages, metal plasmons still suffer from some shortcomings, such as the lack of dynamical tunability, the fabrication cost, and the lack of compatibility with complementary-metal-oxide-semiconductor (CMOS) technology.

3.2. Semiconductor-Based SEIRA

From the perspective of device integration, we need to rely on semiconductors (especially group-IV semiconductors), which additionally can be used to dynamically adjust the resonance frequency through chemical doping or electrical gating. Thus, a wide range of doped semiconductors have been explored as mid-IR plasmonic materials, such as group-IV semiconductors (e.g., Si,[27,122,123] Ge,[28–30] and SiC[77]), group III–V semiconductors (e.g., GaAs,[75,76] InAs,[32,33] InAsSb,[35] GaN,[124] and GaP[125]), and oxide semiconductors (e.g., indium tin oxide (ITO),[71] aluminum-doped zinc oxide (AZO),[126] and gallium-doped zinc oxide[127]). For example, silicon, the most widely used semiconductor, can be highly doped to achieve a free-carrier concentration as high as 10^{20} cm^{-3} using various approaches (e.g., ion implantation)[27,122] that is promising for IR plasmonics. The Drude model provides a good way of estimating the IR plasmonic properties of the doped semiconductors, using parameters extracted from the measured long-wavelength IR optical constants,[27,128] which, for Si with a 10^{20} cm^{-3} doping density, predicts the existence of plasmons beyond 6 µm. Additionally, the small carrier density compared with noble metals leads to a plasmon confinement at the doped Si interface that is 10 times better than that of Au long-IR wavelengths.[27] Furthermore, the tunability of the carrier density in semiconductors offers additional freedom for plasmon engineering, such as, for example, lateral control of carrier concentration in doped Si, which has been shown to enable confined mid-IR plasmons on flat Si surface without requiring nanolithography to nanostructure.[128] Biomedical and chemical sensors utilizing SPPs in the mid-IR range have been developed based on highly doped Si.[129]

In contrast to Si, doped Ge has a smaller effective electron mass (cf. $m^* \approx 0.12$ for Ge[29] and $m^* \approx 0.26$ for Si[130]), leading to a higher plasma frequency for a given doping level, according to Equation (1). Additionally, Ge can be grown epitaxially with great quality (thus contributing to displaying improved plasmon performance), a method that is compatible with Si-based CMOS technology, and therefore amenable to integration in compact microchips.[28,29,31,131] As an example, heavily doped (2.3×10^{19} cm^{-3} carrier density) Ge antennas (1 µm thick, 800 nm width, and 300 nm gap) have been fabricated on an Si substrate and demonstrated to sustain plasmons at 13 µm optical wavelength.[29] Also, epitaxially grown Ge SEIRA antennas have been demonstrated for sensing, showing a signal enhancement of the order of two orders of magnitude at hotspots (see **Figure 5**a).[56]

Group III–V compound semiconductors have also been studied for mid-IR plasmonic applications.[132,133] In particular, some of these materials have significantly smaller effective masses than those of group-IV materials (e.g., Si and Ge), such as GaAs ($m^* \approx 0.09$)[134] and InAs ($m^* \approx 0.04$),[134] therefore reaching the plasmon frequencies of interest with smaller doping densities. In this context, heavily doped InAs subwavelength patterns have been shown to support broadband plasmons across a broad range of mid-IR frequencies (5.5–15 µm) by varying the doping density in the 2.7×10^{18} to 7.5×10^{19} cm^{-3} range.[32] Additionally, epitaxially grown Si-doped InAs nanoantennas with lengths smaller than $\lambda_0/20$ have been demonstrated to sense weak vibrational modes (e.g., 810 and 827 cm^{-1} of a PMMA thin film, Figure 5b).[33] In Barho et al.,[35] highly doped InAsSb gratings on a GaSb substrate were proposed to realize highly sensitive SEIRA and sense a thin 200 nm PMMA layer. Other II–V compound semiconductors, such as highly doped $In_{0.53}Ga_{0.47}As/Al_{0.48}In_{0.52}As$[132] and InAs/GaSb[133] heterostructures, have also been used to demonstrate mid-IR plasmons. It is worth noting that GaAs is not well suited for IR plasmonics because the required high n-type doping (10^{19} cm^{-3}) is hard to achieve in films of this material,[41,135] while holes possess comparatively large effective mass and poor mobility.[75]

Transparent conducting oxides such as ITO can have high electron densities exceeding[78] 10^{21} cm^{-3}, which allows them to sustain SPPs with resonance frequencies reaching the near-IR spectral region.[71,127,136] In this context, arrays of ITO plasmonic nanoantennas have been demonstrated for SEIRA (Figure 5c).[78] Interestingly, although the plasmonic intensity enhancement factor by an individual ITO antenna (≈400) is smaller than that of an equivalent Au antenna (≈2000),[9,10] ITO antennas present the advantage that they can be integrated into ultracompact arrays. In ITO, this is made possible by the 3–4-fold increase in the surface-plasmon wavelength compared to Au rods of the same length. This implies that ITO antennas can be made more compact and arranged with a higher packing density, which can be exploited to achieve a high integration density of plasmonic hotspots per unit area, so that ITO antenna arrays can effectively deliver a similar performance in SEIRA as their noble-metal counterparts (see enhanced vibrational spectra in Figure 5c). By reducing the distance of spaced antenna arrays, near-field plasmonic coupling between the antennas can be activated, largely enhancing the achieved enhancement, as previously demonstrated in metal-based IR

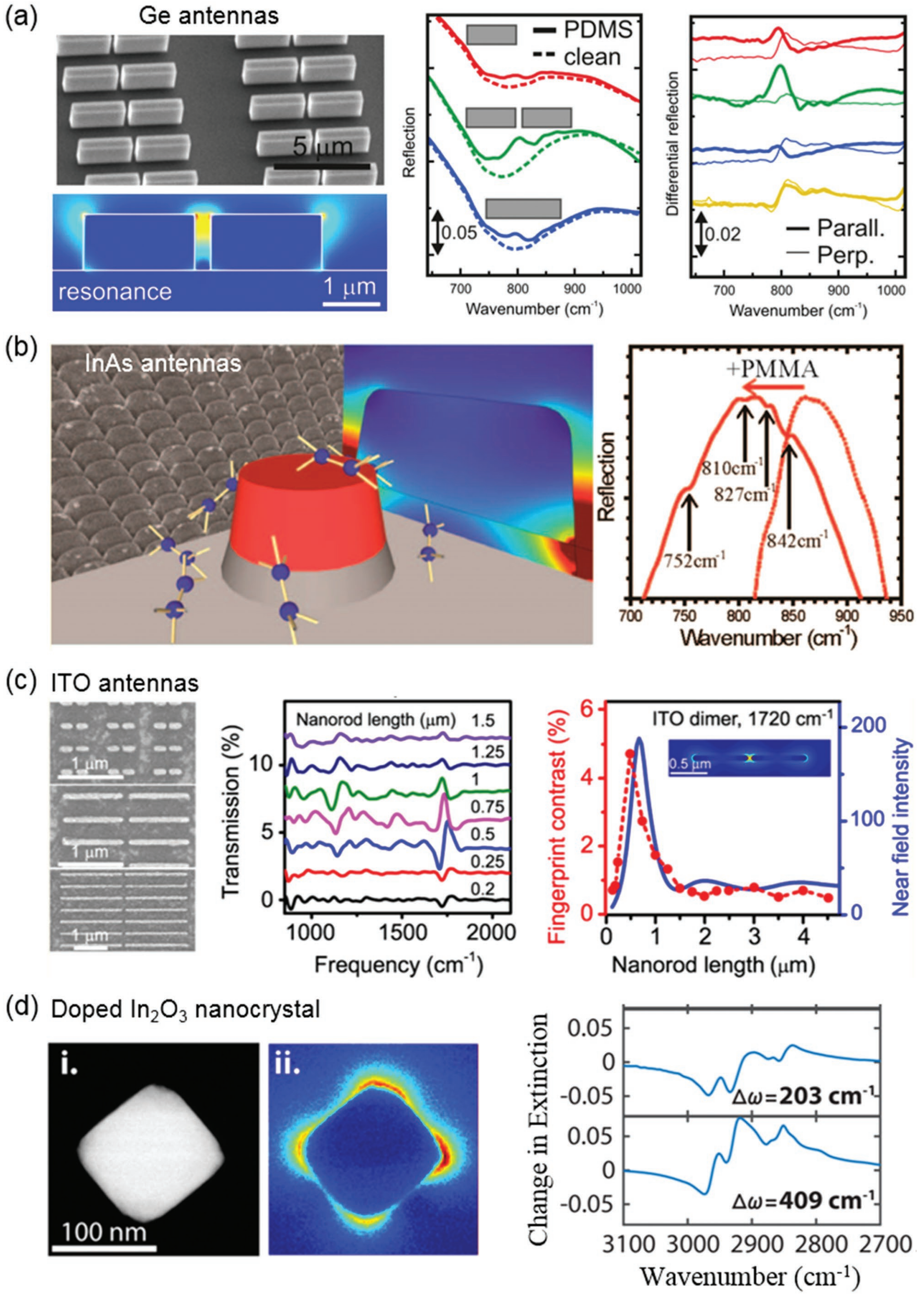

Figure 5. SEIRA based on semiconductor plasmons. a) Ge antennas. Left: SEM image (top) and simulated plasmonic near-field intensity enhancement (bottom) of Ge antennas on Si. Middle: Reflection spectra of three antenna samples before (dashed curves) and after (solid curves) PDMS film coating. Right: The vibrational mode response extracted from reflection spectra in the middle panel.[56] b) InAs antennas. Left: Schematic, SEM image and calculated electric-field intensities of InAs nanoantennas.[33] Right: Reflection spectra of the InAs antennas before and after coating with a 50 nm thick PMMA layer. c) ITO antennas. Left: SEM images of ITO antennas with different lengths. Middle: Extracted vibrational mode response based on ITO antennas. Right: Fingerprint contrast obtained by taking the peak-to-peak amplitude of the mode at a frequency of 1720 cm^{-1} (red, left axis) and calculated near-field intensity taken at the center of the antenna gap (blue, right axis). Inset: Electric-field-intensity map of an ITO dimer antenna.[78] d) In_2O_3 nanocrystal. Left and middle: A plasmon resonance mode mapped by EELS performed using a scanning transmission electron microscope on a nanocrystal at 0.62 eV/5000 cm^{-1}. Right: Extracted vibrational mode response based on nanocrystals with varied doping concentration.[137] a) Reproduced with permission.[56] Copyright 2015, American Chemical Society. b) Reproduced with permission.[33] Copyright 2013, American Chemical Society. c) Reproduced with permission.[78] Copyright 2014, American Chemical Society. d) Reproduced with permission.[137] Copyright 2017, American Chemical Society.

plasmonics (Figure 5c).[10,108] Colloidal cubic nanocrystals of F and Sn co-doped In_2O_3 have also been exploited for SEIRA.[137] Actually, these structures display strong plasmon-driven near-field enhancement that has been directly mapped through electron energy-loss spectroscopy (EELS) (see Figure 5d) and optically probed through FTIR measurements. Based on these results, the vibrational features of monolayer oleate ligands bounded to these nanocrystals were clearly detected on the extinction spectra, as shown in Figure 5d (right plot).[137] Other oxide semiconductors, such as heavily doped ZnO (e.g., Ga:ZnO),[138] 2D VO_2 nanosquare arrays,[37] ITO single nanocrystals and AZO single nanocrystals,[139] have also been demonstrated to support plasmons in a broad mid-IR spectral range.

The above examples show that the doping concentration of semiconductors can be tuned by several orders of magnitude, resulting in a significant tunability of their plasmonic properties. However, the key limitation of semiconductor-based SEIRA is that the carrier mobility in conventional semiconductors is typically too low to support plasmons with low damping at high carrier density[73,74,82,140] (see Figure 2), thus limiting their potential for SEIRA.

3.3. Graphene-Based SEIRA

Recently, graphene has emerged as a promising candidate for mid-IR plasmonic applications.[22–25,141] This monolayer of carbon atoms arranged in a honeycomb lattice exhibits a unique electronic structure characterized by two inequivalent Dirac cones (linear electronic dispersion) at the K and K′ points of the first Brillouin zone (see **Figure 6**a (left)). Electrons in graphene behave as massless Dirac fermions with forbidden backscattering, leading to the highest measured mobility at room temperature (≈200 000 $cm^2\ V^{-1}\ s^{-1}$ in suspended samples[65]). The optical conductivity of pristine graphene, $\sigma = e^2/4\hbar$, produces a spectrally flat absorbance $\pi\alpha = 2.3\%$, where $\alpha = \frac{e^2}{4\pi\hbar\varepsilon_0} = 1/137$ is the fine-structure constant; this result has been experimentally confirmed over the visible and near-IR domains.[142] When doping, the absorption spectra of graphene becomes more interesting. As an example, Figure 6a (right) illustrates a characteristic absorption spectrum of graphene at finite doping,[143] revealing different optical transition processes: the spectral weight described by the Drude response is due to intraband free-carrier absorption; at near-IR and visible frequencies, absorption is produced by direct interband transitions; in the near-IR regime, Pauli blocking limits optical losses, with an observed residual absorption dominated by disorder.[144]

Additionally, when it is highly doped, graphene can support low-energy plasmons that exhibit a number of important features:[24,143,145] they are electrical tunable and can be spectrally modulated over wide frequency regions in the mid-IR; their wavelength is several orders of magnitude smaller than the light wavelength at the same frequency; and they are long lived. Some of these properties are summarized by the relation

$$\frac{\lambda_p}{\lambda_0} \approx \frac{2\alpha}{\varepsilon_1 + \varepsilon_2} \frac{E_F}{\hbar\omega} \tag{9}$$

between the plasmon and light wavelengths λ_p and λ_0, where E_F is the Fermi energy relative to the neutrality point, $\hbar\omega$ is the photon energy, and ε_1 and ε_2 are the permittivities of the media on either side of the graphene layer. For typical Fermi energies, about 0.1–1 eV, photon energies in the mid-IR, and dielectric environment with moderate permittivities, the above equation predicts that λ_p is two orders of magnitude smaller than λ_0. Such an extremely high optical confinement renders graphene as an attractive platform for mid-IR plasmon-enhanced sensing.

A side effect of their extreme optical confinement is that radiative damping can be neglected in graphene plasmons, although unfortunately, this also means that light couples rather inefficiently to these excitations. Nonetheless, the level of near-field enhancement can reach unprecedentedly high values.[146]

Figure 6b,c illustrates how the graphene plasmon resonance frequency can be tuned electrically, as well as by structural design. By exploiting this possibility, it has been shown that graphene plasmons can potentially enable SEIRA to cover the whole mid-IR spectral range, as well as the terahertz spectral range by in situ tuning.[23,67,143]

Different sources of plasmon damping have been extensively explored in graphene.[43,67,147] However, in large-scale chemical vapor deposited graphene, impurity and defect scattering is the dominant source of damping, limiting the plasmon lifetime to ≈100 fs at most.

Importantly, although there is no fundamental reason preventing the frequency of graphene plasmons to reach up to the visible, in practice the experimental results so far reported are limited to the mid-IR range, with plasmons observed at light wavelengths in the range from ~3 µm to several tens of micrometers.

The optical response associated with graphene plasmons is highly sensitive to the nature of the supporting substrate. For example, the carrier mobility drops significantly when graphene is placed on an insulating dielectric (e.g., SiO_2) due to efficient carrier scattering by surface phonons and charged impurities.[148] Therefore, the choice of substrate is of great importance for low-loss graphene plasmonics, and in this respect, hBN has been shown to provide an optimum choice for encapsulation.[43] When the plasmon energy becomes comparable with that of the substrate's polar phonons, hybridization between plasmons and phonons occurs.[149] This is neatly illustrated by the strong plasmon–phonon coupling observed in graphene nanoribbons supported on SiO_2 substrates.[67,150,151] The plasmonic resonance peak then splits into multiple peaks. Additionally, when two different dielectrics are involved, plasmon–phonon coupling becomes more complex,[150–152] as shown for the hBN/graphene/SiO_2 heterostructure, in which four resonant peaks are observed in the extinction spectra (Figure 6d,e), resulting from the strong coupling of graphene plasmons, a surface optical phonon in SiO_2 (1168 cm^{-1}) and two optical phonons in hBN (820 and 1370 cm^{-1}). We understand that the strong coupling between graphene plasmons and substrate phonons indicates that this material can be very sensitive to the molecular vibrational signals that one targets in SEIRA (see Section 2.2).

The unique properties of graphene plasmons that we have briefly reviewed above are excellent attributes for SEIRA applications (see also Section 2). Next, we summarize some notable aspects of graphene-based SEIRA.

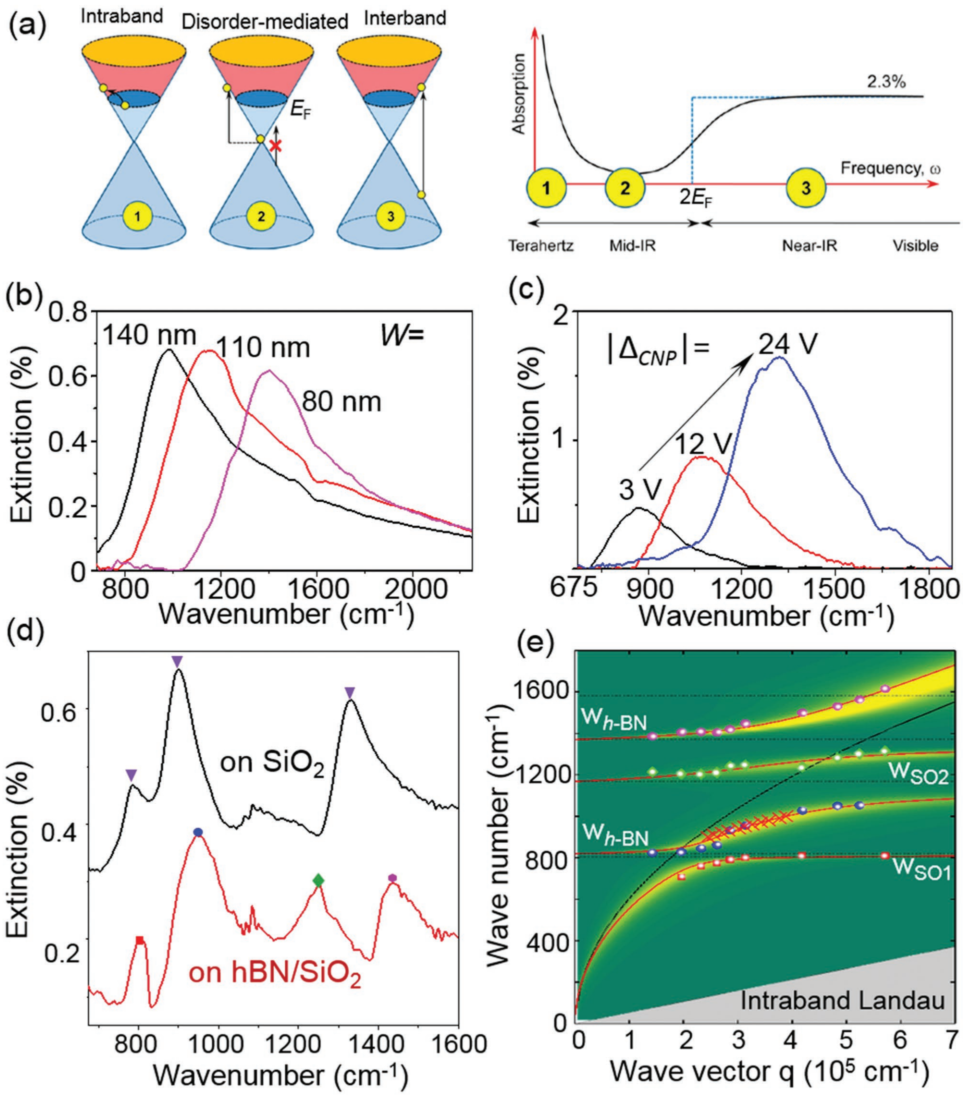

Figure 6. Graphene plasmons. a) Illustration of a typical absorption spectrum of doped graphene and the corresponding optical transition processes.[143] E_F is the Fermi level of graphene. Extinction spectra of graphene nanoribbons showing a plasmon resonance and its evolution with b) ribbon width W and c) gate voltage. Δ_{CNP} is the effective gate voltage. The spectra are obtained from graphene nanoribbon arrays on 300 nm CaF_2/Si. d) Plasmonic response in graphene/SiO_2 and hBN/graphene/SiO_2 heterostructures.[150] e) Dispersion of graphene plasmons in an hBN/graphene/SiO_2 heterostructure.[150] The red curves correspond to calculated values. The colored dots and crosses represent experimental results. The calculated loss function is plotted as a pseudocolor background. The black curve represents the plasmon dispersion in pristine graphene. a) Reproduced with permission.[143] Copyright 2014, American Chemical Society.

3.3.1. Ultrahigh Sensitivity

The extremely large electromagnetic-field confinement (down to a volume ≈10^6 smaller than the diffraction limit[24]) and long carrier relaxation time of graphene plasmons enable ultrahigh sensitivity detection. In Li et al.,[47] molecular signals emerging as fine features in the graphene plasmon resonant peaks were observed with a fivefold signal enhancement by detecting the C=O bonding of an 8 nm thick PMMA overlayer. Mid-IR plasmonic biosensing with graphene was also demonstrated.[4] Specifically, the plasmon resonance of nanostructured graphene on a Si/SiO_2 substrate was dynamically tuned via the gate voltage to selectively probe the protein at different frequencies (**Figure 7**a). Graphene plasmons demonstrated a superior sensitivity in the detection of both changes in the neighboring refractive index and the molecular vibrational modes of nanometer-thin biomolecules, which introduced frequency shifts exceeding 200 cm^{-1}. Additionally, amide-I and II bands of the sampled protein were revealed in the plasmonic spectra despite the low amount of analyte present in the sample. In particular, for the amide-I band, the graphene plasmonic sensor featured a signal modulation of 27% (Figure 7b), which was almost three times larger than that observed with a gold plasmonic sensor (11%).[4] Such high enhancement is due to the strong field confinement of graphene plasmons in the IR range. For example, with graphene plasmons, over 90% of the mode energy is confined within a 15 nm distance from the graphene surface, whereas the same percentage spreads over a distance of 500 nm

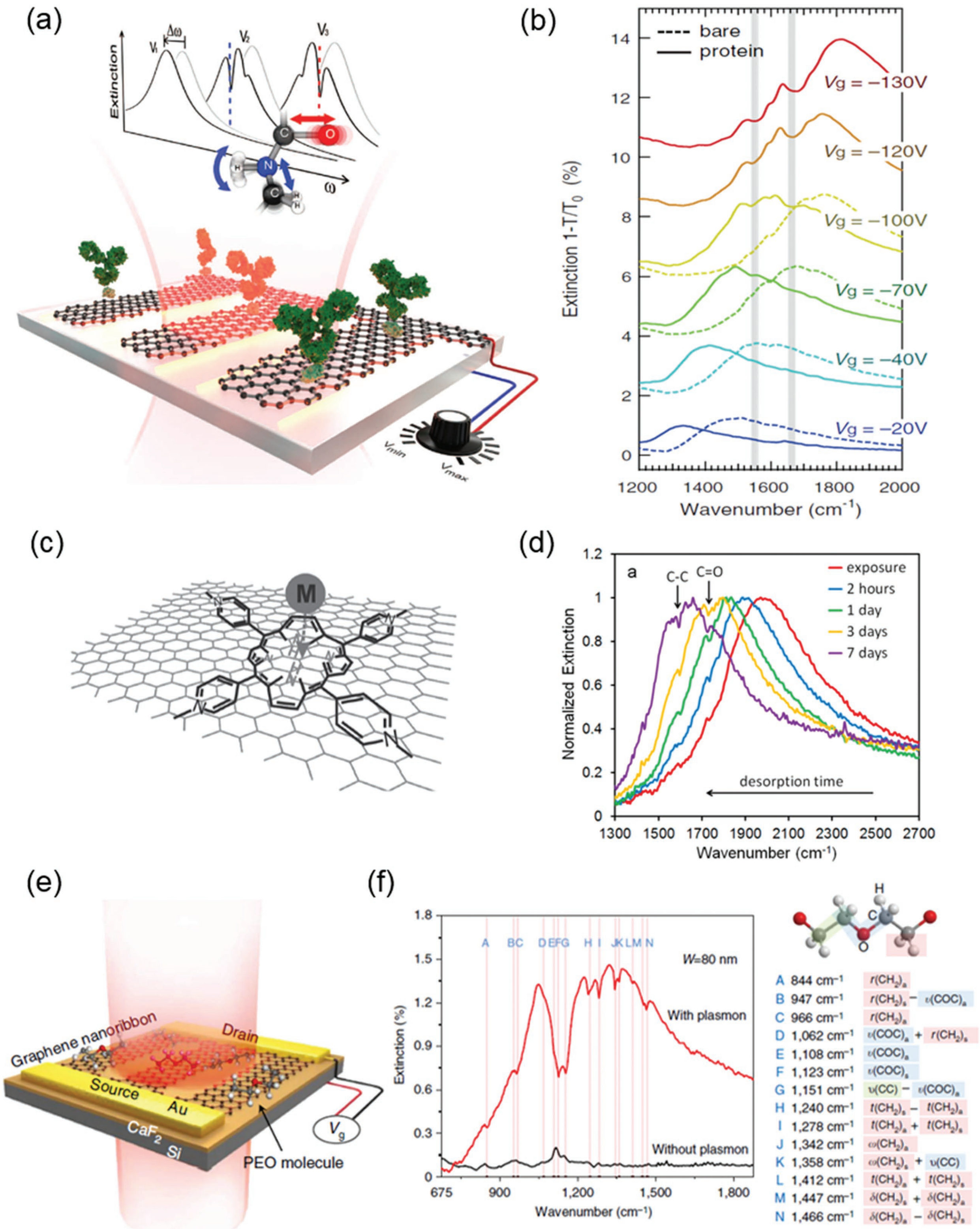

Figure 7. SEIRA based on graphene plasmons. a) Graphene–plasmon biosensor.[4] The presence of proteins produces a plasmon resonance spectral shift ($\Delta\omega$) accompanied by narrow dips corresponding to the molecular vibration bands of the protein. The latter is used for sensing. b) Extinction spectra of a graphene nanoribbon array for different gate voltages (V_g) before (dashed curves) and after (solid curves) protein bilayer formation.[4] c) Metal-ion detection based on graphene plasmons.[154] d) Gas sensing with graphene plasmons.[153] e) Graphene–plasmon sensor in the molecular-fingerprint region.[46] f) Molecular mode fingerprinting of an 8 nm thick PEO film with (red curve) and without (black curve) plasmon enhancement. The red vertical lines indicate various PEO molecular vibrational modes as listed on the right.[46] a,b) Reproduced with permission.[4] Copyright 2017, The American Association for the Advancement of Science. d) Reproduced with permission.[153] Copyright 2016, American Chemical Society. e,f) Reproduced with permission.[46] Copyright 2016, Springer Nature.

away from the gold surface when using gold plasmons.[48] The highest sensitivity was typically obtained when the plasmon frequency was electrically tuned to the molecular modes.[4,46] The discovery that π–π interaction between certain molecules and graphene can further enhance the coupling between the plasmons and related molecular vibrations (such as the C–C breathing mode of perylene-3,4,9,10-tetracarboxylic dianhydride), leading to higher sensitivity, was reported in Farmer et al.[153]

Metal ions and gas molecules have also been detected by graphene plasmon sensors.[153] The detection of metal ions (such as Cd^{2+}, Cu^{2+}, Ca^{2+}, and Zn^{2+}) with graphene plasmons was performed based on nanorods fabricated via a block copolymer self-assembly method.[154] In that study, molecular cages that can bind with ions (e.g., *meta*-5,10,15,20-tetrakis(1-methyl-4-pyridinio)porphyrin tetra(*p*-toluenesulfonate), TMPyP) were absorbed on the graphene surface via electrostatic and π–π stacking interactions (Figure 7c). This led to the significantly sensitive detection of the vibrational modes of TMPyP, which varied with a different combination of ions. The self-assembly method[154] used in that work and other similar methods for device fabrication (such as nanosphere lithography[155]) are cost-effective and readily scalable to fabricate large-area graphene nanostructures for SEIRA applications. Using graphene as a plasmonic sensing platform, acetone and hexane vapor down to 50 zeptomol μm^{-2} have been detected as well (Figure 7d).[153]

Theoretical studies further indicate the great potential of graphene plasmons to detect trace molecules with ultrahigh sensitivity.[49,89,156,157] For example, a recent study reveals that individual elementary charges or a weak dipole can be sufficient to trigger observable modifications in the linear absorption spectra and the nonlinear response of single graphene nanoislands. These results predict ultrasensitive detection of dipolar molecules and molecular radicals, made possible by the extraordinary optoelectronic properties of graphene.[158]

3.3.2. Dynamic Tunability

In contrast to Raman spectroscopy, IR spectroscopy operates over a wide spectral range (from 4 to 25 µm). Dynamically tunable plasmons are highly desirable for SEIRA because the signal enhancement generally decreases with the detuning between the plasmons and the vibrational frequencies (see Section 2.2).[47] In this respect, it is difficult to tune metal plasmons once the geometry is determined. Phase-change materials like VO_2 and $Ge_3Sb_2Te_6$ (GST),[159] which have dielectric functions within the IR spectral range that vary by large amounts when changing phase, have been used as tunable dielectric environments to modulate the plasmon resonance frequency through thermal annealing or by employing ultrafast laser pulses. For example, the dielectric function of GST can be tuned from 12 to 36 when the material transitions from its amorphous phase to the crystalline phase, which can shift the plasmon resonance frequency over several hundred wavenumbers.[159] In contrast, plasmon modulation in graphene can be performed by electrically tuning the carrier density, allowing dynamic control over the plasmon frequency within a continuous range, so that it can be aimed at the targeted molecular vibrational modes of the analytes.[46] This property enables selective sensing over a broad spectral range with a single device.

3.3.3. Molecular Fingerprinting

The molecular-fingerprint spectral region (from 600 to 1500 cm^{-1} or ≈6–16 µm) includes complex vibrational characteristics of molecules in bulk materials, which can be effectively distinguished to enable unambiguous identification. However, all the above-mentioned graphene sensors[4,47,48,153,154] are limited to the spectral range larger than 1200 cm^{-1} due, in part, to the strong coupling between graphene plasmons and the surface optical phonons when using SiO_2 substrates, which are the most common dielectric substrate. Unfortunately, other typical dielectric substrates, such as hBN and SiC, also have strong optical phonons in the technologically important IR fingerprint region. As a promising candidate, diamond-like carbon films do not have phonon modes in this range and can be used as substrates for molecular fingerprinting.[67]

CaF_2 is also transparent in the molecular-fingerprint region. Actually, in Hu et al.[46] graphene–plasmon sensors have been demonstrated using a 300 nm thick CaF_2 nanofilm as a dielectric substrate for molecular fingerprinting at the nanoscale level (Figure 7e). This CaF_2 film is an excellent IR-window substrate, which provides a constant low background in the range of 600–6000 cm^{-1}, and can also be used as a dielectric material for highly efficient electrical doping. For example, the graphene carrier density can be tuned up to 2.6×10^{12} cm^{-2} with a relatively low gate voltage of ≈20 V for a film thickness of 300 nm, and the corresponding plasmon resonance peak can be swapped across the 900–1400 cm^{-1} region. Different graphene structures (e.g., ribbons of varied widths) exhibit plasmons that can cover the whole molecular-fingerprinting region.[46] Using this approach, it has been demonstrated that all 14 IR-active vibrational modes of an 8 nm thick poly(ethylene oxide) (PEO) film in the molecular fingerprinting wavelength region can be effectively resolved with an enhancement factor up to 20 (Figure 7f). Note that the signal enhancement factor can be tuned in situ with gating, which allows it to be adjusted from 2.5 to 23 when the gate voltage is tuned from −6 to −21 V for selective sensing.

3.3.4. Omnidirectional Enhancement

Molecular vibrational modes are typically invisible when the incident light is polarized perpendicular to the molecule vibrational direction. An omnidirectional sensor could address this challenge, which is of great interest for various applications, such as sensing of well-aligned molecules. The omnidirectional and ultrasensitive sensing capability with graphene plasmons was theoretically proposed by utilizing hybridized modes, as described in Liu and Cubukcu.[89] Additionally, in Hu et al.,[46] the simultaneous detection of in-plane and out-of-plane vibrational modes by graphene–plasmon sensors was experimentally demonstrated. In particular, this study focused on out-of-plane modes (also denoted as ZO modes), which are not typically visible in conventional IR microscopy; using monolayer hBN as an example, the plasmonic enhanced IR spectra show both in-plane and out-of-plane vibrational modes at ≈1370 and 820 cm^{-1}, respectively. Omnidirectional sensing with graphene plasmons opens up new possibilities of detecting molecular vibrational modes that cannot be detected with traditional IR spectroscopy.

3.3.5. Spectrometer-Free SEIRA

There is a one-to-one correspondence between the doping level (i.e., the Fermi energy) and the plasmon frequency of well-characterized graphene nanostructures. Therefore, the level of doping can play a similar role for the selection of wavelength as a spectrometer in SEIRA. Using this principle, a theoretical study[157] has predicted the possibility of resolving the spectral features of IR vibrational modes by using a stable broadband light source and monitoring the changes in the overall absorption as a function of doping, varied through a gated device. Although still unrealized in practice, this approach would provide a highly integrated way of detecting and spectrally fingerprinting an analyte without the involvement of a bulky IR spectrometer.

In general, graphene plasmons are highly confined and electrically tunable, which means that they can be used for sensing over a wide spectral range. At the same time, the limited resonant strength (i.e., the weak light absorption inherited from a low carrier density) is a problem that hinders its applications in SEIRA. For example, it is difficult to be combined with SEIRA measurements under internal reflection, which averts the possibility of in vivo measurement. Additionally, the ultrahigh confinement implies that the detection is effective only when the analyte is in close proximity to the sensors. On the positive side, this also means that graphene can reach a higher level of sensitivity (i.e., similar SEIRA features with a smaller amount of analyte).

3.4. Carbon-Nanotube-Based SEIRA

Carbon nanotubes are 1D close relatives of graphene[160,161] and can be viewed as graphene ribbons rolled into seamless cylinders. In addition to the intrinsic plasmons that appear at high energies (>5 eV),[162] CNTs can support longitudinal plasmons at IR frequencies due to the addition of extra charge carriers.[163] Similar to graphene, the carrier density can be tuned either chemically or electrostatically.[164] The generally linear electron dispersion in CNTs implies that their resonance is readily tunable by doping. In addition, the CNT plasmon frequency can be tuned by simply changing the tube length.[165]

Because of their 1D character, CNTs have the ability to confine light down to very small volumes, leading to large Purcell factors.[166] The direct observation of plasmons in single-walled CNTs (SWCNTs) has been reported in Shi et al.[39] at IR wavelengths via scattering scanning near-field optical microscopy (s-SNOM), as shown in **Figure 8**a,b, and further explained in terms of Luthinger's theory. The plasmons in metallic SWCNTs exhibited a remarkable combination of strong spatial confinement and high quality factor, two key figures of merit for plasmonics.[39] Therefore CNTs could be an excellent material for SEIRA. An important issue that has limited progress in this direction is the inhomogeneity (different chirality and lengths) of available CNT samples. This leads to loss of coherence, broad spectra, and low quality factor (Q << 1). However, this limitation has been partially overcome[38] using pure semiconducting nanotubes, aligning them using the Langmuir–Schaeffer technique, transferring them onto SiO_2, and cutting them lithographically to desired lengths (Figure 8c). The resulting thin films composed of CNTs were doped chemically and sampled through FTIR, which yielded spectra revealing that the plasmon frequency was tunable throughout the mid-IR range (up to 3000 cm^{-1}). This approach led to plasmon Q-factors up to 10 and Purcell factors of 10^5. Resonant enhancements were observed for both the 1590 cm^{-1} C–C mode of the CNTs, which is commonly IR-inactive, and the SiO_2 substrate mode at about 1000 cm^{-1}.[38] Plasmon–phonon coupling was also revealed by the observation of anticrossings and transparency dips in the modes as a function of doping, as shown in Figure 8d. In a more recent study involving films composed of aligned CNTs of uniform length L (Figure 8e), it was shown that the plasmon frequencies ν_p were a function of the film thickness t and showed the scaling $\nu_p^2 L \propto t$.[167] This result allows the tuning of CNT plasmons to be extended down to 1.4 µm, as shown in Figure 8f. Moreover, the CNTs' plasmon peak attenuation largely increased for increased thickness, reaching a value of 70%, thus offering an exciting platform for SEIRA.[167] Further improvements in the quality of nanotube samples and tube alignment may lead to new, powerful SEIRA sensors.

3.5. Other Potential SEIRA Materials

Topological insulators can support plasmons over a wide spectral region, from the terahertz to the ultraviolet spectral range.[70,168] For example, micrometer-sized Bi_2Se_3-thin-film gratings exhibit Dirac plasmons sustained by their 2D surface-state electrons, as experimentally observed in the terahertz region (**Figure 9**a).[70] It has been reported that the plasmon linewidth changes surprisingly little with temperatures in the 6–300 K range.[70] Although plasmons in topological insulators have not been directly observed in the IR range, they can be expected because the plasmon frequency can be adjusted by changing the width and period of the grating structure[169] and the chemical composition.[170] It was also theoretically predicted that the interaction of topological insulators and dipole emitters (i.e., molecular vibrations) can be very strong.[171] These results suggest that topological insulators could possibly be used as materials for SEIRA based on tunable IR plasmons.

Superconductors have negative permittivity at low frequencies and can support low-loss plasmons due to their high conductivity.[63,64,93,172] For example, a type-I niobium-sputtered superconductor film has been successfully used to fabricate microwave metamaterials operating at 5 GHz with significantly low losses (1.6×10^{-13} Ω m), roughly five orders of magnitude smaller than those of silver.[173] Negative refraction in a multilayer stack of ferromagnetic and superconducting thin films has also been reported (Figure 9c).[174] Importantly, plasmons in superconductors can be actively tuned through varying the temperature, applying electrical and magnetic fields and via photoexcitation. Figure 9d shows plasmonic-resonance switching and frequency tuning of a high-temperature superconducting

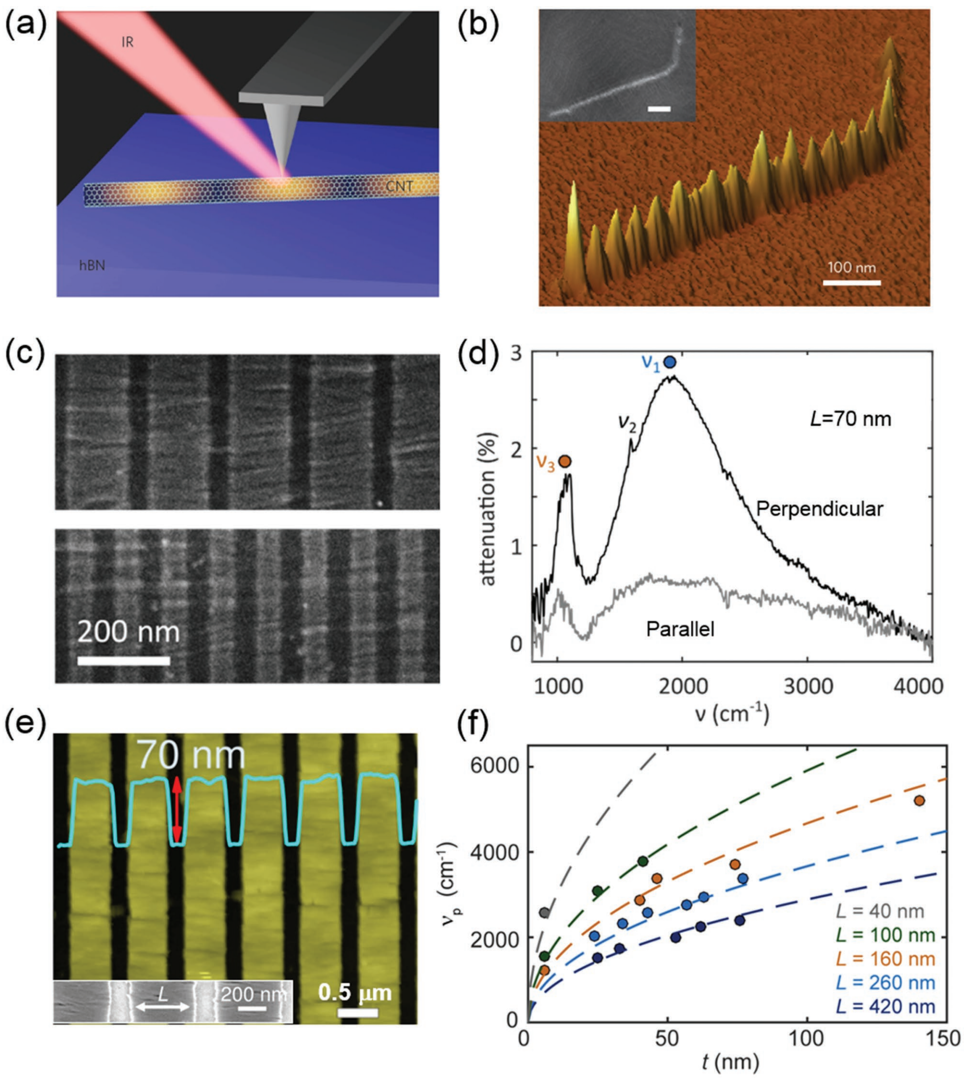

Figure 8. SEIRA based on CNT plasmons. a) Illustration of s-SNOM characterization of plasmons in CNTs.[39] b) 3D plot of the near-field scattering intensity of a plasmon in an SWCNT.[39] c) Aligned CNT segments with varied lengths.[38] d) Spectra showing plasmons excited in CNTs (ν_1) and plasmons coupled to SiO_2-substrate phonons (ν_2 and ν_3) for segments cut perpendicular (parallel) to their alignment direction.[38] e) Typical AFM image of aligned CNT segments with thickness ranging from 25 to 250 nm. Inset: SEM image.[167] f) Plasmon resonance frequency ν_p plotted as a function of CNT film thickness t for different segment lengths L.[167] a,b) Reproduced with permission.[39] Copyright 2017, Springer Nature. c,d) Reproduced with permission.[38] Copyright 2017, American Physical Society. e,f) Reproduced with permission.[167] Copyright 2017, American Chemical Society.

YBCO structure with varying temperature in the terahertz range.[63] However, plasmons supported by superconductors are limited to the microwave domain for niobium-based materials. Photons with higher frequency can break up the Cooper pairs that are responsible for the superconducting current transport. It has therefore been suggested that high-temperature superconductors with a much larger bandgap should be used to support low-loss mid-IR plasmons,[175] an area that deserves further investigation and has potential for low-frequency SEIRA.

3.6. Comparison between Different SEIRA Materials

Based on the properties discussed in detail above, it is clear that each different type of material has specific advantages and limitations. These properties are summarized and contrasted in **Table 1**.

4. Challenges and Opportunities

SEIRA has experienced a rapid development in the past few decades, particularly with the advent of nanostructuring capabilities (e.g., gold nanoantennas) and new materials (e.g., graphene). As discussed in Section 3, SEIRA is finding new applications, including ultrahigh, sensitive detection of trace amount of chemicals, biomolecules, ions, and gases. We anticipate that further developments of SEIRA will lead to new exciting opportunities in the short term, some of which are discussed next.

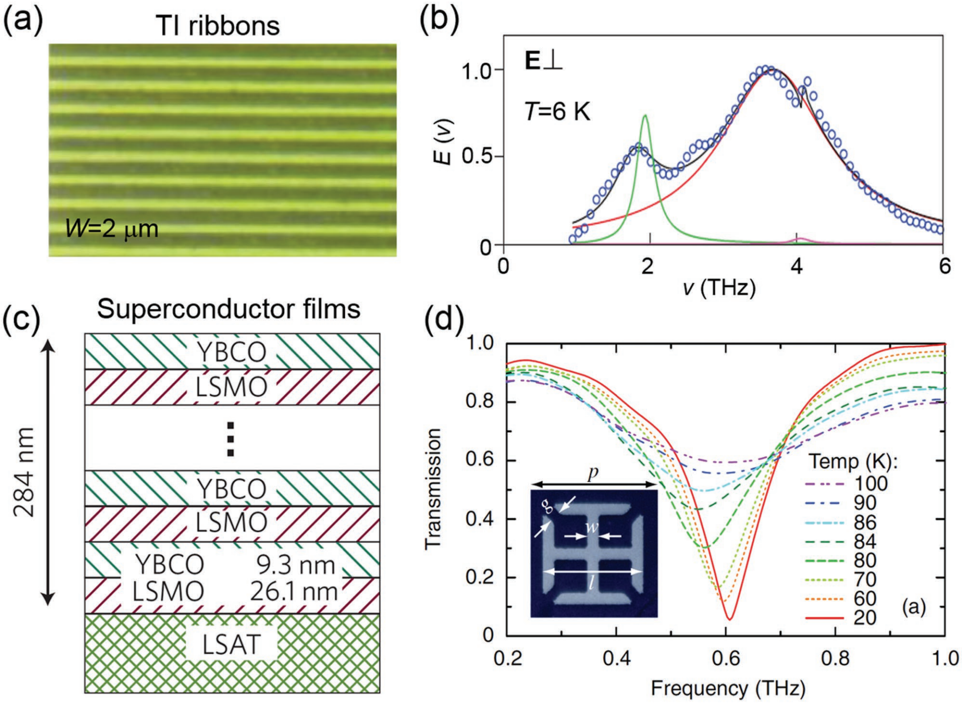

Figure 9. Exotic potential SEIRA materials. a) Bi_2Se_3 topological insulator microstructure (optical microscopy image).[70] TI, topological insulator; *W*, the ribbon width. b) Plasmon (red curve) and phonon (green curve) contributions to the extinction spectrum (circles) for radiation polarized perpendicular to the ribbons in (a), measured at a temperature of 6 K.[70] The black curve is the sum of the red and green curves. c) Superconducting metamaterial nanostructure with negative refractive index.[174] YBCO, yttrium barium copper oxide; LSMO, lanthanum strontium manganese oxide. d) Transmission spectra of YBCO metamaterial at various temperatures.[63] Inset: Optical microscopy image of a single YBCO split-ring resonator. a,b) Reproduced with permission.[70] Copyright 2013, Springer Nature. c) Reproduced with permission.[174] Copyright 2005, American Physical Society. d) Reproduced with permission.[63] Copyright 2017, American Physical Society.

4.1. The Ultimate Detection Limit of SEIRA Spectroscopy: A Case for Graphene Plasmonics

Further improvement in the signal enhancement of SEIRA can have a dramatically positive effect on new and existing applications. For example, there is a great demand for the detection of low contents of proteins in physiological samples (such as cerebral or spinal fluids) with IR techniques. The ability of directly assaying trace molecules and their behavior, such as protein aggregation in real-world biofluids, would therefore entail significant increase in the sensitivity of SEIRA.

The current ultimate limit of IR plasmonic enhancement aims at the direct detection of single atoms and molecules, similar to that which has been achieved in SERS.[176] In this respect, graphene plasmons hold the record field confinement for mid-IR light, combined with strong light–matter interaction, as discussed in Section 3.3. This renders graphene as a promising platform for single-molecule detection via SEIRA. Recent studies have predicted that it is possible to detect a single IR vibrational mode using graphene plasmons.[24,158] For example, Koppens et al.[24] theoretically discussed the interaction between a single quantum emitter and a graphene plasmon, indicating that the extreme mode confinement triggers the ultrafast efficient decay of the quantum emitter into the plasmon in a proximal doped graphene sheet. In Yu et al.,[158] it is suggested that an onset of second-harmonic generation can be produced by doping, in turn resulting from the proximity of polar molecules with respect to otherwise centrosymmetric graphene islands, so that a second-harmonic signal is detected only in the presence of the analytes. The same study also predicted radical changes in the linear absorption spectrum (i.e., SEIRA), raising the possibility of high-sensitivity optical sensors. Experimentally, the design of new structures and the exploration of new and different IR plasmonic materials are still needed to achieve this goal.

4.2. Microfluidic-Based SEIRA

IR spectroscopy has the ability to access molecular fingerprints, as well as to identify different biomolecules such as proteins,[177] lipids,[19] those present in viruses,[178,179] and nucleic acids[180] in a nondestructive and noninvasive manner that is imperative for living biosystems. However, measurement in a liquid environment (e.g., water) is a precondition for studying such systems. The extremely strong absorption of water in the 3000–3600 and 1550–1700 cm^{-1} spectral ranges[181] severely limits the detection sensitivity of IR spectroscopies of biomolecules in its native aqueous environments. Replacing water with other thin layers (around a few micrometers) of solvents, such as hydrophilic methylcellulose, can circumvent this problem.[182] Microfluidics can deliver low amounts of solution for fast and efficient mixing and reaction. Therefore, the combination of FTIR and microfluidics is of significant interest for

Table 1. Comparison between different materials for SEIRA applications (SC: superconductor).

	Advantages	Limitations
Metals	Strong near-field enhancement; compatible with transmittance and reflection measurements; easy to combine with fluids for electrochemistry, biomolecule attachment, etc.	Large damping in the mid-IR; low spatial confinement; no dynamical tunability; not CMOS compatible; high cost.
Semiconductors	Compatible with CMOS technology; tunable spectral range through doping; antennas are more compact than metallic ones.	Large damping from the low carrier mobility; limited doping concentration.
Graphene	Ultrahigh confinement, implying strong light–matter interaction; large electrooptical tunability; ultrahigh mobility (low damping); ultrathin biocompatible impermeable films.	Low carrier concentration; low performance in reflection; high cost; hard to be integrated inside sensing devices (especially for liquid analyte).
CNTs	Ultrahigh confinement; electrooptical tunability; ultrahigh mobility.	Low carrier concentration; complex fabrication.
Others (TI, SC)	Ultrahigh mobility.	SCs are incompatible with mid-IR at room temperature; TIs are fragile and affected by spurious bulk doping.

sensing molecules in living biosystems,[15,183] as well as monitoring dynamical reactions.

There are two key challenges in existing microfluidic systems for sensing small amounts of analytes: the complexity of the system designs (e.g., combining ATR-FTIR with microfluidics to enhance sensitivity) and the low detection sensitivity. It was demonstrated that SEIRA based on leveraging the electromagnetic-field enhancement in the microfluidic channel can further improve the sensitivity for detecting trace amounts of analytes in water. This was shown in experiment for in situ monitoring of proteins and nanoparticle interactions[7] and for capturing the vibrational fingerprints of lipid molecules in aqueous environments in real time.[19] As demonstrated in Figure 4e (Section 3.1), gold antennas fabricated on a CaF_2 substrate, which also acts as IR window, were sealed in a PDMS fluidic chamber for measurement in solution and in situ delivery of the analytes to the sensor.[19] The enhanced IR signal of molecules was recorded via reflectance spectra for real-time monitoring. Note that the SEIRA signal of lipids and protein molecules can also be distinguished in this microfluidic structure.[19]

To further improve the sensitivity, new technology and structures are being anticipated. For example, graphene can be used in a new type of microfluidics setup, which can be combined with nano-FTIR (details in the following section). Furthermore, single-atom-thick graphene can be molded into transporting channels for single molecules (**Figure 10**a),[184] while graphene nanostructures can also support plasmons that amplify the SEIRA signal. This technology may find wide usage in areas such as flow processes, reaction imaging, biochemical reaction monitoring, in vivo cell analysis, and pharmaceutical drug investigations.

4.3. Nano-FTIR-Based SEIRA

The spatial resolution of conventional IR spectroscopy is constrained by the diffraction limit to roughly half the illumination wavelength. However, with an evanescent mode detection strategy, s-SNOM provides an excellent optical resolution down to the 10 nm range, independent of the operation wavelength.[185,186] This is typically based on atomic force microscopy setups in which the tip is illuminated with a focused laser beam and the tip-scattered light is detected simultaneously. Unavoidable background contributions are suppressed by introducing vertical tip oscillations (tapping mode) and subsequently Fourier transforming the detected signal and retaining only high-harmonic components of the periodic modulation. The application potential of nano-FTIR has been demonstrated.[187] For example, nano-FTIR (Figure 10c), based on an s-SNOM equipped with a coherent-continuum infrared light source, has been demonstrated for high-spatial-resolution detection (down to 20 nm).[179,185,188] Nanoscale mapping of a molecular mixture has been demonstrated to obtain high contrast in vibrational absorption for nanoscale polymer identification, as shown in Figure 10d.[179,189] Besides nano-FTIR, photothermally induced resonances (PTIR) can couple with a pulsed wavelength-tunable laser to measure light absorption in the sample by transducing the sample thermal expansion into mechanical cantilever motion.[18,190] This can also provide IR spectra with ≈20 nm spatial resolution.[18,190] The applications of nano-FTIR or PTIR are mainly limited by the relatively weak signals due to an extremely large mismatch between the IR wavelength and the active area beneath the tiny tip (≈15 nm). This can be addressed with plasmonic structures by enhancing the nano-FTIR responses. For example, by modifying the scanning probe, IR-resonant-antenna-based s-SNOM tips can realize IR near-field imaging of tobacco mosaic viruses with a diameter of only 18 nm.[191] Furthermore, the plasmonic structure can also be utilized as a supporting substrate to increase the sensitivity. For example, the combination of resonant gold antennas and graphene plasmons can significantly enhance the signal by up to ≈40 times.[192]

Graphene is also a promising material for this purpose (i.e., to enhance nano-FTIR). Real-space imaging of graphene–plasmon polaritons[25,26] strongly suggests that this material can significantly enhance evanescent fields.[193] Such enhancement can be further improved by ultraconfined plasmonic hotspots, such as graphene nanobubbles.[194] For example, in s-SNOM measurements, monolayer-graphene-based ultrathin superlenses offer a sevenfold enhancement of evanescent modes and help resolve buried structures at a 500 nm depth with $\lambda/11$-resolution.[195] Graphene plasmons can penetrate below the sample surface to enhance and probe the evanescent modes on subsurface and sub-diffraction-limited objects (Figure 10e). Further tunable experiments based upon gating or doping graphene would contribute to facilitate broadband IR spectroscopic applications.

As mentioned above, in vivo IR studies are of great importance for biosystems, but it is hard to implement nano-FTIR

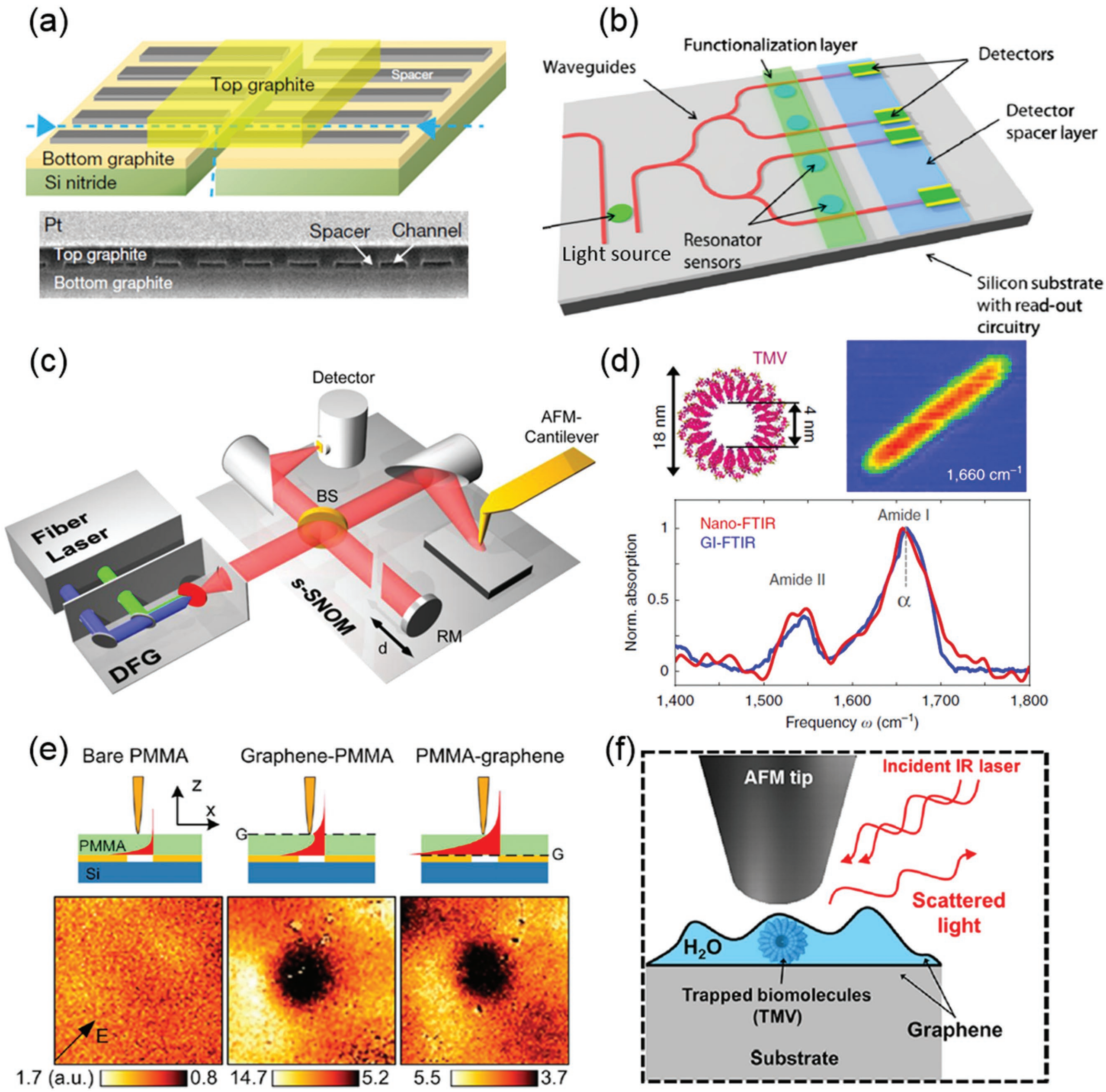

Figure 10. Opportunities for SEIRA. a) Graphene capillaries with atomic-scale precision, which may combine SEIRA with single-molecule transport.[184] b) Schematic of monolithic mid-IR on-chip sensor.[199] c) Schematic of nano-FTIR. Difference-frequency generation (DFG) is used as a mid-IR pump beam. Backscattered light is analyzed with an asymmetric Michelson interferometer comprising a beamsplitter (BS) and a reference mirror (RM).[179] d) IR nanospectroscopy of an individual tobacco mosaic virus.[179] e) Graphene-enhanced near-field microscopy (amplitude images) of a hole buried by a PMMA layer (left), graphene–PMMA (middle), and PMMA–graphene (right).[195] f) Graphene as an impermeable barrier for nano-IR inspection of underlying biomolecules in water.[196] a) Reproduced with permission.[174] Copyright 2016, Springer Nature. b) Reproduced with permission.[189] Copyright 2013, Open Access. c,d) Reproduced with permission.[169] Copyright 2013, Springer Nature. e) Reproduced with permission.[185] Copyright 2014, American Chemical Society. f) Reproduced with permission.[186] Copyright 2015, American Chemical Society.

in liquids due to both the strong absorption of water and the difficulties associated with the dynamics of operating an atomic force microscope in tapping mode inside fluids.[196] Graphene is the thinnest possible membrane that is both impermeable and conductive,[181,197] so it can act as a monolayer barrier that allows IR inspection of the underlying molecular materials in relatively thin liquid-layer environments (Figure 10f).[196] Due to all these extraordinary properties, graphene–plasmon-enhanced nano-FTIR is expected to impact a wide range of areas, such as imaging of biochemical reactions, and in vivo cell analysis with ultrahigh spatial resolution. Additionally, the mechanical and impermeability properties of graphene could be exploited to hold thin aqueous samples combined with more traditional approaches to SEIRA near-field enhancement.

4.4. On-Chip Integration of SEIRA

The increasing demand for rapid sensing and diagnosis in remote areas requires the development of compact and cost-effective mid-IR sensing devices.[198] A mid-IR spectrometer typically consists of a broadband thermal emitter and a broad-band detector, external optics and an FTIR spectrometer. It is technologically important to pursue on-chip IR spectroscopy by miniaturizing and integrating these optical components. So far, discrete optical components, such as on-chip light sources, waveguides, and detectors, can be integrated directly within microreactors (Figure 10b).[198,199] A key goal of the integrated mid-IR sensor is to achieve a strong interaction between the analytes and the IR light transmitting on-chip. As discussed in Section 3, plasmons can dramatically enhance the features of IR spectra while decreasing the reaction area. This presents great potential for on-chip integration of SEIRA. For example, in Romeo et al.,[200] a microfluidic platform equipped with a pedestal Si waveguide, an integrated light source, and chalcogenide PbTe planar resonator sensors was developed for mid-IR chip sensing applications. Note that such a silicon-integrated SEIRA system can be further pushed by relying on the advantages of well-developed CMOS technology. In this respect, a demonstration of a monolithically integrated lab-on-a-chip based on mid-IR absorption spectroscopy is presented in Schwarz et al.[198] A bifunctional quantum-cascade laser/detector was used for integrating and downscaling, and an SPP waveguide was used to increase the chemicals' IR signals. The sensor demonstrated the capability of reaching ppm (one part per million) accuracy.[198] Compared with the dielectric waveguide approach, the plasmonic waveguide can largely enhance light–matter interaction, and therefore, it is anticipated that the field of SEIRA analytical chemistry will be expanded toward all-in-one labs on a chip. For example, the on-chip light source has the potential to be made of wide-band tunable quantum-cascade lasers; the detector can be made of wide-band quantum-cascade detectors (e.g., PbTe planar resonator sensors); and the plasmonic waveguide could be composed of tunable graphene or a semiconductor to obtain a wide range of SEIRA responses. Additionally, the realization of nanowaveguides in MoS_2 using s-SNOM may also open the door for integrating IR sensors with the traditional dielectric waveguides at the nanoscale.[186] Furthermore, semiconductors, graphene, and CNTs are compatible with CMOS technology, thus holding great promise for on-chip integrated devices and enabling a large range of emerging applications.

5. Conclusion

We have surveyed the significant progress of SEIRA over the last few years, summarized its current state, and discussed perspectives for future developments. In particular, we have presented a comprehensive discussion on the applicability of various materials (e.g., metals, semiconductors, and graphene) for SEIRA, as well as potential applications in scientific frontiers such as single-molecule detection and in vivo bioassays. Given the extremely fast pace at which developments on new nanomaterials and structures are being studied for SEIRA, we anticipate the emergence of new opportunities for novel applications in areas such as IR astronomy,[201] IR wireless communication,[202] IR quantum photonics,[203] IR nonlinear optics,[161,204] and ultrafast nano-FTIR[205] to name just a few.

Acknowledgements

The authors thank Kaihui Liu for valuable discussion. This work was supported by the National Basic Key Research Program of China (Grant No. 2015CB932400), the National Key Research and Development Program of China (Grant No. 2016YFA0201600), the National Natural Science Foundation of China (Grant Nos. 51372045, 11504063, and 11674073), the key program of the bureau of Frontier Sciences and Education Chinese Academy of Sciences (Grant No. QYZDB-SSW-SLH021), Academy of Finland (Grant Nos. 276376, 284548, 295777, 304666, 312297, 312551, and 314810), TEKES (OPEC), and the European Union's Seventh Framework Programme (REA grant agreement No. 631610). T.L. acknowledges support from the National Science Foundation under Grant No. NSF/EFRI-1741660. F.J.G.A. acknowledges the Spanish MINECO (Grant Nos. MAT2017-88492-R and SEV2015-0522), the Catalan CERCA and AGAUR (2014-SGR-1400) programs, and Fundació Privada Cellex.

Conflict of Interest

The authors declare no conflict of interest.

Keywords

graphene, infrared spectroscopy, nanostructure, plasmons, surface-enhanced spectroscopy

Received: August 26, 2017
Revised: December 5, 2017
Published online: March 23, 2018

[1] B. H. Stuart, *Infrared Spectroscopy: Fundamentals and Applications*, Wiley, Chichester, UK **2005**.
[2] a) A. Bagri, C. Mattevi, M. Acik, Y. J. Chabal, M. Chhowalla, V. B. Shenoy, *Nat. Chem.* **2010**, *2*, 581; b) L. J. Mauer, A. A. Chernyshova, A. Hiatt, A. Deering, R. Davis, *J. Agric. Food Chem.* **2009**, *57*, 3974; c) F. Garczarek, K. Gerwert, *Nature* **2006**, *439*, 109.
[3] M. Osawa, in *Advances in Electrochemical Science and Engineering*, (Eds: R. C. Alkire, D. M. Kolb, J. Lipkowski, P. N. Ross), Vol. *9*, Wiley-VCH, Weinheim, Germany **2006**, Ch. 8.
[4] D. Rodrigo, O. Limaj, D. Janner, D. Etezadi, F. J. García de Abajo, V. Pruneri, H. Altug, *Science* **2015**, *349*, 165.
[5] R. Adato, S. Aksu, H. Altug, *Mater. Today* **2015**, *18*, 436.
[6] J. Kundu, F. Le, P. Nordlander, N. J. Halas, *Chem. Phys. Lett.* **2008**, *452*, 115.
[7] R. Adato, H. Altug, *Nat. Commun.* **2013**, *4*, 2154.
[8] C. Wu, A. B. Khanikaev, R. Adato, N. Arju, A. A. Yanik, H. Altug, G. Shvets, *Nat. Mater.* **2012**, *11*, 69.
[9] F. Neubrech, A. Pucci, T. W. Cornelius, S. Karim, A. García-Etxarri, J. Aizpurua, *Phys. Rev. Lett.* **2008**, *101*, 157403.
[10] R. Adato, A. A. Yanik, J. J. Amsden, D. L. Kaplan, F. G. Omenetto, M. K. Hong, S. Erramilli, H. Altug, *Proc. Natl. Acad. Sci. USA* **2009**, *106*, 19227.

[11] A. Hartstein, J. R. Kirtley, J. C. Tsang, *Phys. Rev. Lett.* **1980**, *45*, 201.
[12] a) M. Osawa, M. Ikeda, *J. Phys. Chem.* **1991**, *95*, 9914; b) T. R. Jensen, R. P. Van Duyne, S. A. Johnson, V. A. Maroni, *Appl. Spectrosc.* **2000**, *54*, 371; c) D. Enders, A. Puccia, *Appl. Phys. Lett.* **2006**, *88*, 184104.
[13] M. Osawa, K. Ataka, K. Yoshii, Y. Nishikawa, *Appl. Spectrosc.* **1993**, *47*, 1497.
[14] H. Miyake, S. Ye, M. Osawa, *Electrochem. Commun.* **2002**, *4*, 973.
[15] R. F. Aroca, D. J. Ross, C. Domingo, *Appl. Spectrosc.* **2004**, *58*, 324A.
[16] a) F. Neubrech, A. Pucci, *IEEE J. Sel. Top. Quantum Electron.* **2013**, *19*, 4600809; b) N. J. Halas, S. Lal, W.-S. Chang, S. Link, P. Nordlander, *Chem. Rev.* **2011**, *111*, 3913.
[17] F. Neubrech, C. Huck, K. Weber, A. Pucci, H. Giessen, *Chem. Rev.* **2017**, *117*, 5110.
[18] A. Dazzi, C. B. Prater, *Chem. Rev.* **2017**, *117*, 5146.
[19] O. Limaj, D. Etezadi, N. J. Wittenberg, D. Rodrigo, D. Yoo, S.-H. Oh, H. Altug, *Nano Lett.* **2016**, *16*, 1502.
[20] a) I. Schubert, C. Huck, P. Kröber, F. Neubrech, A. Pucci, M. E. Toimil-Molares, C. Trautmann, J. Vogt, *Adv. Opt. Mater.* **2016**, *4*, 1838; b) A. Quirk, M. J. Lardner, Z. Tun, I. J. Burgess, *Langmuir* **2016**, *32*, 2225; c) O. Selig, R. Siffels, Y. L. A. Rezus, *Phys. Rev. Lett.* **2015**, *114*, 233004; d) K. Ataka, S. T. Stripp, J. Heberle, *Biochim. Biophys. Acta, Biomembr.* **2013**, *1828*, 2283; e) S. Aksu, A. E. Cetin, R. Adato, H. Altug, *Adv. Opt. Mater.* **2013**, *1*, 798.
[21] E. H. Hwang, S. Das Sarma, *Phys. Rev. B* **2007**, *75*, 205418.
[22] M. Jablan, H. Buljan, M. Soljacic, *Phys. Rev. B* **2009**, *80*, 245435.
[23] L. Ju, B. S. Geng, J. Horng, C. Girit, M. Martin, Z. Hao, H. A. Bechtel, X. G. Liang, A. Zettl, Y. R. Shen, F. Wang, *Nat. Nanotechnol.* **2011**, *6*, 630.
[24] F. H. L. Koppens, D. E. Chang, F. J. García de Abajo, *Nano Lett.* **2011**, *11*, 3370.
[25] J. N. Chen, M. Badioli, P. Alonso-Gonzalez, S. Thongrattanasiri, F. Huth, J. Osmond, M. Spasenovic, A. Centeno, A. Pesquera, P. Godignon, A. Z. Elorza, N. Camara, F. J. García de Abajo, R. Hillenbrand, F. H. L. Koppens, *Nature* **2012**, *487*, 77.
[26] Z. Fei, A. S. Rodin, G. O. Andreev, W. Bao, A. S. McLeod, M. Wagner, L. M. Zhang, Z. Zhao, M. Thiemens, G. Dominguez, M. M. Fogler, A. H. C. Neto, C. N. Lau, F. Keilmann, D. N. Basov, *Nature* **2012**, *487*, 82.
[27] J. C. Ginn, R. L. Jarecki, E. A. Shaner, P. S. Davids, *J. Appl. Phys.* **2011**, *110*, 043110.
[28] M. P. Fischer, C. Schmidt, E. Sakat, J. Stock, A. Samarelli, J. Frigerio, M. Ortolani, D. J. Paul, G. Isella, A. Leitenstorfer, P. Biagioni, D. Brida, *Phys. Rev. Lett.* **2016**, *117*, 047401.
[29] A. Samarelli, J. Frigerio, E. Sakat, L. Baldassarre, K. Gallacher, M. Finazzi, G. Isella, M. Ortolani, P. Biagioni, D. J. Paul, *Thin Solid Films* **2016**, *602*, 52.
[30] W. Li, P. Anantha, S. Bao, K. H. Lee, X. Guo, T. Hu, L. Zhang, H. Wang, R. Soref, C. S. Tan, *Appl. Phys. Lett.* **2016**, *109*, 241101.
[31] J. Frigerio, A. Ballabio, G. Isella, E. Sakat, G. Pellegrini, P. Biagioni, M. Bollani, E. Napolitani, C. Manganelli, M. Virgilio, A. Grupp, M. P. Fischer, D. Brida, K. Gallacher, D. J. Paul, L. Baldassarre, P. Calvani, V. Giliberti, A. Nucara, M. Ortolani, *Phys. Rev. B* **2016**, *94*, 085202.
[32] S. Law, D. C. Adams, A. M. Taylor, D. Wasserman, *Opt. Express* **2012**, *20*, 12155.
[33] S. Law, L. Yu, A. Rosenberg, D. Wasserman, *Nano Lett.* **2013**, *13*, 4569.
[34] S. Law, R. Liu, D. Wasserman, *J. Vac. Sci. Technol. B: Nanotechnol. Microelectron.: Mater., Process., Meas., Phenom.* **2014**, *32*, 052601.
[35] F. B. Barho, F. Gonzalez-Posada, M.-J. Milla-Rodrigo, M. Bomers, L. Cerutti, T. Taliercio, *Opt. Express* **2016**, *24*, 16175.
[36] E. Sachet, C. T. Shelton, J. S. Harris, B. E. Gaddy, D. L. Irving, S. Curtarolo, B. F. Donovan, P. E. Hopkins, P. A. Sharma, A. L. Sharma, J. Ihlefeld, S. Franzen, J.-P. Maria, *Nat. Mater.* **2015**, *14*, 414.
[37] H. Matsui, Y.-L. Ho, T. Kanki, H. Tanaka, J.-J. Delaunay, H. Tabata, *Adv. Opt. Mater.* **2015**, *3*, 1759.
[38] A. L. Falk, K.-C. Chiu, D. B. Farmer, Q. Cao, J. Tersoff, Y.-H. Lee, P. Avouris, S.-J. Han, *Phys. Rev. Lett.* **2017**, *118*, 257401.
[39] Z. Shi, X. Hong, H. A. Bechtel, B. Zeng, M. C. Martin, K. Watanabe, T. Taniguchi, Y.-R. Shen, F. Wang, *Nat. Photonics* **2015**, *9*, 515.
[40] a) Y. Zhong, S. D. Malagari, T. Hamilton, D. Wasserman, *J. Nanophotonics* **2015**, *9*, 093791; b) R. Stanley, *Nat. Photonics* **2012**, *6*, 409.
[41] G. V. Naik, V. M. Shalaev, A. Boltasseva, *Adv. Mater.* **2013**, *25*, 3264.
[42] a) K. S. Novoselov, A. K. Geim, S. V. Morozov, D. Jiang, Y. Zhang, S. V. Dubonos, I. V. Grigorieva, A. A. Firsov, *Science* **2004**, *306*, 666; b) K. S. Novoselov, A. K. Geim, S. V. Morozov, D. Jiang, M. I. Katsnelson, I. V. Grigorieva, S. V. Dubonos, A. A. Firsov, *Nature* **2005**, *438*, 197.
[43] A. Woessner, M. B. Lundeberg, Y. Gao, A. Principi, P. Alonso-González, M. Carrega, K. Watanabe, T. Taniguchi, G. Vignale, M. Polini, J. Hone, R. Hillenbrand, F. H. L. Koppens, *Nat. Mater.* **2015**, *14*, 421.
[44] a) A. N. Grigorenko, M. Polini, K. S. Novoselov, *Nat. Photonics* **2012**, *6*, 749; b) V. W. Brar, M. S. Jang, M. Sherrott, J. J. Lopez, H. A. Atwater, *Nano Lett.* **2013**, *13*, 2541.
[45] L. Novotny, *Phys. Rev. Lett.* **2007**, *98*, 266802.
[46] H. Hu, X. Yang, F. Zhai, D. Hu, R. Liu, K. Liu, Z. Sun, Q. Dai, *Nat. Commun.* **2016**, *7*, 12334.
[47] Y. Li, H. Yan, D. B. Farmer, X. Meng, W. Zhu, R. M. Osgood, T. F. Heinz, P. Avouris, *Nano Lett.* **2014**, *14*, 1573.
[48] I. J. Luxmoore, P. Q. Liu, P. Li, J. Faist, G. R. Nash, *ACS Photonics* **2016**, *3*, 936.
[49] Y. Cui, A. Lauchner, A. Manjavacas, F. J. Garcia de Abajo, N. J. Halas, P. Nordlander, *Nano Lett.* **2016**, *16*, 6390.
[50] Q. Guo, C. Li, B. Deng, S. Yuan, F. Guinea, F. Xia, *ACS Photonics* **2017**, *4*, 2989.
[51] D. Dregely, F. Neubrech, H. Duan, R. Vogelgesang, H. Giessen, *Nat. Commun.* **2013**, *4*, 2237.
[52] N. W. Ashcroft, N. D. Mermin, *Solid State Physics*, Harcourt College Publishers, New York **1976**.
[53] S. D. Sarma, E. H. Hwang, *Phys. Rev. Lett.* **2009**, *102*, 206412.
[54] P. Johnson, R. Christy, *Phys. Rev. B* **1972**, *6*, 4370.
[55] J. W. Cleary, R. E. Peale, D. J. Shelton, G. D. Boreman, C. W. Smith, M. Ishigami, R. Soref, A. Drehman, W. R. Buchwald, *J. Opt. Soc. Am. B* **2010**, *27*, 730.
[56] L. Baldassarre, E. Sakat, J. Frigerio, A. Samarelli, K. Gallacher, E. Calandrini, G. Isella, D. J. Paul, M. Ortolani, P. Biagioni, *Nano Lett.* **2015**, *15*, 7225.
[57] T. Low, A. Chaves, J. D. Caldwell, A. Kumar, N. X. Fang, P. Avouris, T. F. Heinz, F. Guinea, L. Martin-Moreno, F. Koppens, *Nat. Mater.* **2017**, *16*, 182.
[58] F. J. García de Abajo, *ACS Photonics* **2014**, *1*, 135.
[59] A. Boltasseva, H. A. Atwater, *Science* **2011**, *331*, 290.
[60] M. G. Blaber, M. D. Arnold, M. J. Ford, *J. Phys. Chem. C* **2009**, *113*, 3041.
[61] E. J. Zeman, G. C. Schatz, *J. Phys. Chem.* **1987**, *91*, 634.
[62] M. A. Ordal, R. J. Bell, R. W. Alexander, L. L. Long, M. R. Querry, *Appl. Opt.* **1985**, *24*, 4493.
[63] H.-T. Chen, H. Yang, R. Singh, J. F. O'Hara, A. K. Azad, S. A. Trugman, Q. X. Jia, A. J. Taylor, *Phys. Rev. Lett.* **2010**, *105*, 247402.
[64] J. Philipp, V. U. Alexey, M. A. Steven, *Supercond. Sci. Technol.* **2014**, *27*, 073001.

[65] X. Du, I. Skachko, A. Barker, E. Y. Andrei, *Nat. Nanotechnol.* **2008**, *3*, 491.
[66] C. R. Dean, A. F. Young, I. Meric, C. Lee, L. Wang, S. Sorgenfrei, K. Watanabe, T. Taniguchi, P. Kim, K. L. Shepard, J. Hone, *Nat. Nanotechnol.* **2010**, *5*, 722.
[67] H. G. Yan, T. Low, W. J. Zhu, Y. Q. Wu, M. Freitag, X. S. Li, F. Guinea, P. Avouris, F. N. Xia, *Nat. Photonics* **2013**, *7*, 394.
[68] X. Yang, X.-T. Kong, B. Bai, Z. Li, H. Hu, X. Qiu, Q. Dai, *Small* **2015**, *11*, 6.
[69] J. N. Hancock, J. L. M. van Mechelen, A. B. Kuzmenko, D. van der Marel, C. Brüne, E. G. Novik, G. V. Astakhov, H. Buhmann, L. W. Molenkamp, *Phys. Rev. Lett.* **2011**, *107*, 136803.
[70] P. Di Pietro, M. Ortolani, O. Limaj, A. Di Gaspare, V. Giliberti, F. Giorgianni, M. Brahlek, N. Bansal, N. Koirala, S. Oh, P. Calvani, S. Lupi, *Nat. Nanotechnol.* **2013**, *8*, 556.
[71] S. H. Brewer, S. Franzen, *J. Phys. Chem. C* **2002**, *106*, 12986.
[72] S. Kalusniak, L. Orphal, P. Schäfer, S. Sadofev, *Phys. Status Solidi B* **2016**, *253*, 361.
[73] L. E. Vorobyev, in *Handbook Series on Semiconductor Parameters*, Vol. *1*, World Scientific, Singapore **1996**, Ch. 2.
[74] M. E. Levinshtein, S. L. Rumyantsev, in *Handbook Series on Semiconductor Parameters*, Vol. *1*, World Scientific, Singapore **1996**, Ch. 1.
[75] W. Songprakob, R. Zallen, W. K. Liu, K. L. Bacher, *Phys. Rev. B* **2000**, *62*, 4501.
[76] a) R. Matz, H. Lüth, *Phys. Rev. Lett.* **1981**, *46*, 500; b) A. Mooradian, G. B. Wright, *Phys. Rev. Lett.* **1966**, *16*, 999.
[77] W. Du, F. Zhao, *Mater. Lett.* **2014**, *115*, 92.
[78] M. Abb, Y. Wang, N. Papasimakis, C. H. de Groot, O. L. Muskens, *Nano Lett.* **2014**, *14*, 346.
[79] A. E. Krasnok, I. S. Maksymov, A. I. Denisyuk, P. A. Belov, A. E. Miroshnichenko, C. R. Simovski, Y. S. Kivshar, *Phys.-Usp* **2013**, *56*, 539.
[80] C. Sönnichsen, T. Franzl, T. Wilk, G. von Plessen, J. Feldmann, O. Wilson, P. Mulvaney, *Phys. Rev. Lett.* **2002**, *88*, 077402.
[81] a) J. Lermé, *J. Phys. Chem. C* **2011**, *115*, 14098; b) K. Kolwas, A. Derkachova, *J. Quant. Spectrosc. Radiat. Transfer* **2013**, *114*, 45.
[82] M. E. Levinshtein, S. L. Rumyantsev, in *Handbook Series on Semiconductor Parameters*, Vol. *1*, World Scientific, Singapore **1996**, Ch. 4.
[83] L. Novotny, *Am. J. Phys.* **2010**, *78*, 1199.
[84] C. L. Garrido Alzar, M. A. G. Martinez, P. Nussenzveig, *Am. J. Phys.* **2002**, *70*, 37.
[85] H. Yan, T. Low, F. Guinea, F. Xia, P. Avouris, *Nano Lett.* **2014**, *14*, 4581.
[86] T. Low, F. Guinea, H. Yan, F. Xia, P. Avouris, *Phys. Rev. Lett.* **2014**, *112*, 116801.
[87] V. Giannini, Y. Francescato, H. Amrania, C. C. Phillips, S. A. Maier, *Nano Lett.* **2011**, *11*, 2835.
[88] U. Fano, *Phys. Rev.* **1961**, *124*, 1866.
[89] F. Liu, E. Cubukcu, *Phys. Rev. B* **2013**, *88*, 115439.
[90] A. Priebe, M. Sinther, G. Fahsold, A. Pucci, *J. Chem. Phys.* **2003**, *119*, 4887.
[91] a) H. D. Lutz, G. Schneider, G. Kliche, *J. Phys Chem Solids* **1985**, *46*, 437; b) M. Osawa, K.-i. Ataka, *Surf. Sci.* **1992**, *262*, L118.
[92] a) P. Ge, Z. H. Zhou, *Proc. Natl. Acad. Sci. USA* **2011**, *108*, 9637; b) H. Pfnur, C. Tegenkamp, L. Vattuone, arXiv:1701.05049 **2017**.
[93] T. Anagnostis, A. F. Vassili, F. J. García de Abajo, I. Z. Nikolay, *New. J. Phys.* **2012**, *14*, 115006.
[94] M. Osawa, K.-I. Ataka, K. Yoshii, Y. Nishikawa, *Appl. Spectrosc.* **1993**, *47*, 1497.
[95] K. Ataka, J. Heberle, *Anal. Bioanal. Chem.* **2007**, *388*, 47.
[96] a) A. Hatta, Y. Chiba, W. Suëtaka, *Appl. Surf. Sci.* **1986**, *25*, 327; b) M. Osawa, K. Yoshii, *Appl. Spectrosc.* **1997**, *51*, 512.
[97] H. Wang, J. Kundu, N. J. Halas, *Angew. Chem., Int. Ed.* **2007**, *46*, 9040.
[98] F. Le, D. W. Brandl, Y. A. Urzhumov, H. Wang, J. Kundu, N. J. Halas, J. Aizpurua, P. Nordlander, *ACS Nano* **2008**, *2*, 707.
[99] J. V. Coe, K. R. Rodriguez, S. Teeters-Kennedy, K. Cilwa, J. Heer, H. Tian, S. M. Williams, *J. Phys. Chem. C* **2007**, *111*, 17459.
[100] P. Muhlschlegel, H. J. Eisler, O. J. F. Martin, B. Hecht, D. W. Pohl, *Science* **2005**, *308*, 1607.
[101] a) M. Schnell, A. Garcia Etxarri, A. J. Huber, K. Crozier, J. Aizpurua, R. Hillenbrand, *Nat. Photonics* **2009**, *3*, 287; b) F. Neubrech, T. Kolb, R. Lovrincic, G. Fahsold, A. Pucci, J. Aizpurua, T. W. Cornelius, M. E. Toimil-Molares, R. Neumann, S. Karim, *Appl. Phys. Lett.* **2006**, *89*, 253104.
[102] A. Pucci, F. Neubrech, D. Weber, S. Hong, T. Toury, M. L. de la Chapelle, *Phys. Status Solidi B* **2010**, *247*, 2071.
[103] P. Alonso-González, P. Albella, M. Schnell, J. Chen, F. Huth, A. García-Etxarri, F. Casanova, F. Golmar, L. Arzubiaga, L. E. Hueso, J. Aizpurua, R. Hillenbrand, *Nat. Commun.* **2012**, *3*, 684.
[104] a) K. B. Crozier, A. Sundaramurthy, G. S. Kino, C. F. Quate, *J. Appl. Phys.* **2003**, *94*, 4632; b) F. Neubrech, D. Weber, R. Lovrincic, A. Pucci, M. Lopes, T. Toury, M. Lamy de La Chapelle, *Appl. Phys. Lett.* **2008**, *93*, 163105.
[105] a) T. Neuman, C. Huck, J. Vogt, F. Neubrech, R. Hillenbrand, J. Aizpurua, A. Pucci, *J. Phys. Chem. C* **2015**, *119*, 26652; b) R. Adato, A. Artar, S. Erramilli, H. Altug, *Nano Lett.* **2013**, *13*, 2584; c) P. Alonso-González, P. Albella, F. Neubrech, C. Huck, J. Chen, F. Golmar, F. Casanova, L. E. Hueso, A. Pucci, J. Aizpurua, R. Hillenbrand, *Phys. Rev. Lett.* **2013**, *110*, 203902.
[106] J. H. Klein-Wiele, P. Simon, H. G. Rubahn, *Phys. Rev. Lett.* **1998**, *80*, 45.
[107] a) R. Adato, A. A. Yanik, C.-H. Wu, G. Shvets, H. Altug, *Opt. Express* **2010**, *18*, 4526; b) F. Neubrech, S. Beck, T. Glaser, M. Hentschel, H. Giessen, A. Pucci, *ACS Nano* **2014**, *8*, 6250.
[108] S. Aksu, A. A. Yanik, R. Adato, A. Artar, M. Huang, H. Altug, *Nano Lett.* **2010**, *10*, 2511.
[109] a) L. Rayleigh, *London, Edinburgh, Dublin Philos. Mag. J. Sci.* **1907**, *14*, 60; b) F. J. García de Abajo, *Rev. Mod. Phys.* **2007**, *79*, 1267.
[110] S. Cataldo, J. Zhao, F. Neubrech, B. Frank, C. Zhang, P. V. Braun, H. Giessen, *ACS Nano* **2012**, *6*, 979.
[111] E. Cubukcu, S. Zhang, Y. S. Park, G. Bartal, X. Zhang, *Appl. Phys. Lett.* **2009**, *95*, 043113.
[112] K. Chen, R. Adato, H. Altug, *ACS Nano* **2012**, *6*, 7998.
[113] Y. Li, L. Su, C. Shou, C. Yu, J. Deng, Y. Fang, *Sci. Rep.* **2013**, *3*, 2865.
[114] A. Tittl, A.-K. U. Michel, M. Schäferling, X. Yin, B. Gholipour, L. Cui, M. Wuttig, T. Taubner, F. Neubrech, H. Giessen, *Adv. Mater.* **2015**, *27*, 4597.
[115] L. V. Brown, K. Zhao, N. King, H. Sobhani, P. Nordlander, N. J. Halas, *J. Am. Chem. Soc.* **2013**, *135*, 3688.
[116] P. Biagioni, J. S. Huang, B. Hecht, *Rep. Prog. Phys.* **2012**, *75*, 024402.
[117] I. M. Pryce, Y. A. Kelaita, K. Aydin, H. A. Atwater, *ACS Nano* **2011**, *5*, 8167.
[118] a) M. A. Kats, R. Blanchard, P. Genevet, Z. Yang, M. M. Qazilbash, D. N. Basov, S. Ramanathan, F. Capasso, *Opt. Lett.* **2013**, *38*, 368; b) K. Chen, T. Duy Dao, T. Nagao, *Sci. Rep.* **2017**, *7*, 44069.
[119] A. G. Milekhin, O. Cherkasova, S. A. Kuznetsov, I. A. Milekhin, E. E. Rodyakina, A. V. Latyshev, S. Banerjee, G. Salvan, D. R. T. Zahn, *Beilstein J. Nanotechnol.* **2017**, *8*, 975.
[120] C. D'Andrea, J. Bochterle, A. Toma, C. Huck, F. Neubrech, E. Messina, B. Fazio, O. M. Maragò, E. Di Fabrizio, M. Lamy de La Chapelle, P. G. Gucciardi, A. Pucci, *ACS Nano* **2013**, *7*, 3522.
[121] D. Etezadi, J. B. Warner Iv, F. S. Ruggeri, G. Dietler, H. Lashuel, H. Altug, *Light: Sci. Appl.* **2017**, *6*, e17029.

[122] M. Shahzad, G. Medhi, R. E. Peale, W. R. Buchwald, J. W. Cleary, R. Soref, G. D. Boreman, O. Edwards, *J. Appl. Phys.* **2011**, *110*, 123105.
[123] L.-W. Chou, N. Shin, S. V. Sivaram, M. A. Filler, *J. Am. Chem. Soc.* **2012**, *134*, 16155.
[124] a) A. Stolz, L. Considine, S. Faci, E. Dogheche, C. Tripon-Canseliet, B. Loiseaux, D. Pavlidis, D. Decoster, J. Chazelas, *Opt. Lett.* **2012**, *37*, 3039; b) T. Kozawa, T. Kachi, H. Kano, Y. Taga, M. Hashimoto, N. Koide, K. Manabe, *J. Appl. Phys.* **1994**, *75*, 1098.
[125] K. Ishioka, K. Brixius, U. Höfer, A. Rustagi, E. M. Thatcher, C. J. Stanton, H. Petek, *Phys. Rev. B* **2015**, *92*, 205203.
[126] G. V. Naik, J. Kim, A. Boltasseva, *Opt. Mater. Express* **2011**, *1*, 1090.
[127] M. A. Noginov, L. Gu, J. Livenere, G. Zhu, A. K. Pradhan, R. Mundle, M. Bahoura, Y. A. Barnakov, V. A. Podolskiy, *Appl. Phys. Lett.* **2011**, *99*, 021101.
[128] R. Aaron, S. Joshua, L. Runyu, S. William, L. Stephanie, L. S. Leslie, B. Rohit, W. Daniel, *J. Opt.* **2014**, *16*, 094012.
[129] Y.-B. Chen, *Opt. Express* **2009**, *17*, 3130.
[130] M. Miyao, T. Motooka, N. Natsuaki, T. Tokuyama, *Solid State Commun.* **1981**, *37*, 605.
[131] a) L. Baldassarre, E. Calandrini, A. Samarelli, K. Gallacher, D. J. Paul, J. Frigerio, G. Isella, E. Sakat, M. Finazzi, P. Biagioni, M. Ortolani, presented at 39th Int. Conf. on Infrared, Millimeter, and Terahertz Waves, AZ, September **2014**; b) P. Biagioni, J. Frigerio, A. Samarelli, K. Gallacher, L. Baldassarre, E. Sakat, E. Calandrini, R. W. Millar, V. Giliberti, G. Isella, D. J. Paul, M. Ortolani, *J. Nanophotonics* **2015**, *9*, 093789.
[132] A. J. Hoffman, L. Alekseyev, S. S. Howard, K. J. Franz, D. Wasserman, V. A. Podolskiy, E. E. Narimanov, D. L. Sivco, C. Gmachl, *Nat. Mater.* **2007**, *6*, 946.
[133] D. Li, C. Z. Ning, *Opt. Express* **2011**, *19*, 14594.
[134] M. Cardona, *Phys. Rev.* **1961**, *121*, 752.
[135] J. H. Neave, P. J. Dobson, J. J. Harris, P. Dawson, B. A. Joyce, *Appl. Phys. A* **1983**, *32*, 195.
[136] a) C. Rhodes, M. Cerruti, A. Efremenko, M. Losego, D. E. Aspnes, J.-P. Maria, S. Franzen, *J. Appl. Phys.* **2008**, *103*, 093108; b) S. Q. Li, P. Guo, L. Zhang, W. Zhou, T. W. Odom, T. Seideman, J. B. Ketterson, R. P. H. Chang, *ACS Nano* **2011**, *5*, 9161; c) H. Caglayan, S.-H. Hong, B. Edwards, C. R. Kagan, N. Engheta, *Phys. Rev. Lett.* **2013**, *111*, 073904.
[137] A. Agrawal, A. Singh, S. Yazdi, A. Singh, G. K. Ong, K. Bustillo, R. W. Johns, E. Ringe, D. J. Milliron, *Nano Lett.* **2017**, *17*, 2611.
[138] a) S. Kalusniak, S. Sadofev, F. Henneberger, *Phys. Rev. Lett.* **2014**, *112*, 137401; b) J. Kim, G. V. Naik, A. V. Gavrilenko, K. Dondapati, V. I. Gavrilenko, S. M. Prokes, O. J. Glembocki, V. M. Shalaev, A. Boltasseva, *Phys. Rev. X* **2013**, *3*, 041037.
[139] R. W. Johns, H. A. Bechtel, E. L. Runnerstrom, A. Agrawal, S. D. Lounis, D. J. Milliron, *Nat. Commun.* **2016**, *7*, 11583.
[140] Y. A. Goldberg, in *Handbook Series on Semiconductor Parameters*, Vol. *1*, World Scientific, Singapore **2012**, Ch. 9.
[141] a) C. H. Gan, H. S. Chu, E. P. Li, *Phys. Rev. B* **2012**, *85*, 125431; b) F. D'Apuzzo, A. R. Piacenti, F. Giorgianni, M. Autore, M. C. Guidi, A. Marcelli, U. Schade, Y. Ito, M. Chen, S. Lupi, *Nat. Commun.* **2017**, *8*, 14885; c) Z. Sun, A. Martinez, F. Wang, *Nat. Photonics* **2016**, *10*, 227; d) X. Guo, H. Hu, X. Zhu, X. Yang, Q. Dai, *Nanoscale* **2017**, *9*, 14998.
[142] a) R. R. Nair, P. Blake, A. N. Grigorenko, K. S. Novoselov, T. J. Booth, T. Stauber, N. M. R. Peres, A. K. Geim, *Science* **2008**, *320*, 1308; b) H. Hu, B. Liao, X. Guo, D. Hu, X. Qiao, N. Liu, R. Liu, K. Chen, B. Bai, X. Yang, Q. Dai, *Small* **2017**, *13*, 1603812.
[143] T. Low, P. Avouris, *ACS Nano* **2014**, *8*, 16.
[144] Z. Q. Li, E. A. Henriksen, Z. Jiang, Z. Hao, M. C. Martin, P. Kim, H. L. Stormer, D. N. Basov, *Nat. Phys.* **2008**, *4*, 532.
[145] H. Hu, F. Zhai, D. Hu, Z. Li, B. Bai, X. Yang, Q. Dai, *Nanoscale* **2015**, *7*, 19493.
[146] S. Thongrattanasiri, F. J. García de Abajo, *Phys. Rev. Lett.* **2013**, *110*, 187401.
[147] A. Principi, G. Vignale, M. Carrega, M. Polini, *Phys. Rev. B* **2013**, *88*, 195405.
[148] J.-H. Chen, C. Jang, S. Xiao, M. Ishigami, M. S. Fuhrer, *Nat. Nanotechnol.* **2008**, *3*, 206.
[149] E. H. Hwang, R. Sensarma, S. Das Sarma, *Phys. Rev. B* **2010**, *82*, 195406.
[150] X. Yang, F. Zhai, H. Hu, D. Hu, R. Liu, S. Zhang, M. Sun, Z. Sun, J. Chen, Q. Dai, *Adv. Mater.* **2016**, *28*, 2931.
[151] V. W. Brar, M. S. Jang, M. Sherrott, S. Kim, J. J. Lopez, L. B. Kim, M. Choi, H. Atwater, *Nano Lett.* **2014**, *14*, 3876.
[152] R. Liu, B. Liao, X. Guo, D. Hu, H. Hu, L. Du, H. Yu, G. Zhang, X. Yang, Q. Dai, *Nanoscale* **2017**, *9*, 208.
[153] D. B. Farmer, P. Avouris, Y. Li, T. F. Heinz, S.-J. Han, *ACS Photonics* **2016**, *3*, 553.
[154] K. Zhang, L. Zhang, F. L. Yap, P. Song, C. W. Qiu, K. P. Loh, *Small* **2016**, *12*, 1302.
[155] X. Zhu, W. Wang, W. Yan, M. B. Larsen, P. Bøggild, T. G. Pedersen, S. Xiao, J. Zi, N. A. Mortensen, *Nano Lett.* **2014**, *14*, 2907.
[156] T. Wu, L. Wei, *Opt. Express* **2016**, *24*, 26241.
[157] A. Marini, I. Silveiro, F. J. García de Abajo, *ACS Photonics* **2015**, *2*, 876.
[158] R. Yu, J. D. Cox, F. J. García de Abajo, *Phys. Rev. Lett.* **2016**, *117*, 123904.
[159] a) A.-K. U. Michel, D. N. Chigrin, T. W. W. Maß, K. Schönauer, M. Salinga, M. Wuttig, T. Taubner, *Nano Lett.* **2013**, *13*, 3470; b) A.-K. U. Michel, P. Zalden, D. N. Chigrin, M. Wuttig, A. M. Lindenberg, T. Taubner, *ACS Photonics* **2014**, *1*, 833.
[160] a) T. W. Odom, J.-L. Huang, P. Kim, C. M. Lieber, *Nature* **1998**, *391*, 62; b) M. S. Dresselhaus, G. Dresselhaus, R. Saito, A. Jorio, *Phys. Rep.* **2005**, *409*, 47.
[161] C. Li, X. Zhou, F. Zhai, Z. Li, F. Yao, R. Qiao, K. Chen, M. T. Cole, D. Yu, Z. Sun, K. Liu, Q. Dai, *Adv. Mater.* **2017**, *29*, 1701580.
[162] C. Kramberger, T. Thurakitseree, S. Maruyama, M. Knupfer, *Nanotechnology* **2013**, *24*, 405202.
[163] a) G. Y. Slepyan, S. A. Maksimenko, A. Lakhtakia, O. Yevtushenko, A. V. Gusakov, *Phys. Rev. B* **1999**, *60*, 17136; b) T. Nakanishi, T. Ando, *J. Phys. Soc. Jpn.* **2009**, *78*, 114708.
[164] P. Avouris, Z. Chen, V. Perebeinos, *Nat. Nanotechnol.* **2007**, *2*, 605.
[165] T. Morimoto, S.-K. Joung, T. Saito, D. N. Futaba, K. Hata, T. Okazaki, *ACS Nano* **2014**, *8*, 9897.
[166] L. Martín-Moreno, F. J. García de Abajo, F. J. García-Vidal, *Phys. Rev. Lett.* **2015**, *115*, 173601.
[167] K.-C. Chiu, A. L. Falk, P.-H. Ho, D. B. Farmer, G. Tulevski, Y.-H. Lee, P. Avouris, S.-J. Han, *Nano Lett.* **2017**, *17*, 5641.
[168] a) M. Autore, F. D'Apuzzo, A. Di Gaspare, V. Giliberti, O. Limaj, P. Roy, M. Brahlek, N. Koirala, S. Oh, F. J. García de Abajo, S. Lupi, *Adv. Opt. Mater.* **2015**, *3*, 1257; b) S. Sim, H. Jang, N. Koirala, M. Brahlek, J. Moon, J. H. Sung, J. Park, S. Cha, S. Oh, M.-H. Jo, J.-H. Ahn, H. Choi, *Nat. Commun.* **2015**, *6*, 9814.
[169] J.-Y. Ou, J.-K. So, G. Adamo, A. Sulaev, L. Wang, N. I. Zheludev, *Nat. Commun.* **2014**, *5*, 5139.
[170] W. S. Whitney, V. W. Brar, Y. Ou, Y. Shao, A. R. Davoyan, D. N. Basov, K. He, Q.-K. Xue, H. A. Atwater, *Nano Lett.* **2017**, *17*, 255.
[171] J. Qi, H. Liu, X. C. Xie, *Phys. Rev. B* **2014**, *89*, 155420.
[172] C. Kurter, J. Abrahams, G. Shvets, S. M. Anlage, *Phys. Rev. B* **2013**, *88*, 180510.
[173] a) S. M. Anlage, *J. Opt.* **2011**, *13*, 024001; b) P. Tassin, T. Koschny, M. Kafesaki, C. M. Soukoulis, *Nat. Photonics* **2012**, *6*, 259.
[174] A. Pimenov, A. Loidl, P. Przyslupski, B. Dabrowski, *Phys. Rev. Lett.* **2005**, *95*, 247009.
[175] N. I. Zheludev, Y. S. Kivshar, *Nat. Mater.* **2012**, *11*, 917.

[176] a) K. Kneipp, Y. Wang, H. Kneipp, L. T. Perelman, I. Itzkan, R. R. Dasari, M. S. Feld, *Phys. Rev. Lett.* **1997**, *78*, 1667; b) A. D. McFarland, R. P. Van Duyne, *Nano Lett.* **2003**, *3*, 1057.
[177] Á. I. López-Lorente, B. Mizaikoff, *Anal. Bioanal. Chem.* **2016**, *408*, 2875.
[178] M. Brehm, T. Taubner, R. Hillenbrand, F. Keilmann, *Nano Lett.* **2006**, *6*, 1307.
[179] I. Amenabar, S. Poly, W. Nuansing, E. H. Hubrich, A. A. Govyadinov, F. Huth, R. Krutokhvostov, L. B. Zhang, M. Knez, J. Heberle, A. M. Bittner, R. Hillenbrand, *Nat. Commun.* **2013**, *4*, 2890.
[180] M. Kakuta, P. Hinsmann, A. Manz, B. Lendl, *Lab Chip* **2003**, *3*, 82.
[181] M. Falk, T. A. Ford, *Can. J. Chem.* **1966**, *44*, 1699.
[182] A. Tsiatmas, A. R. Buckingham, V. A. Fedotov, S. Wang, Y. Chen, P. A. J. de Groot, N. I. Zheludev, *Appl. Phys. Lett.* **2010**, *97*, 111106.
[183] a) D. Prim, S. Crelier, J.-M. Segura, *Chimia* **2011**, *65*, 815; b) A. Sobhani, A. Manjavacas, Y. Cao, M. J. McClain, F. J. García de Abajo, P. Nordlander, N. J. Halas, *Nano Lett.* **2015**, *15*, 6946.
[184] B. Radha, A. Esfandiar, F. C. Wang, A. P. Rooney, K. Gopinadhan, A. Keerthi, A. Mishchenko, A. Janardanan, P. Blake, L. Fumagalli, M. Lozada-Hidalgo, S. Garaj, S. J. Haigh, I. V. Grigorieva, H. A. Wu, A. K. Geim, *Nature* **2016**, *538*, 222.
[185] R. Hillenbrand, T. Taubner, F. Keilmann, *Nature* **2002**, *418*, 159.
[186] D. Hu, X. Yang, C. Li, R. Liu, Z. Yao, H. Hu, S. N. G. Corder, J. Chen, Z. Sun, M. Liu, Q. Dai, *Nat. Commun.* **2017**, *8*, 1471.
[187] F. Keilmann, R. Hillenbrand, *Philos. Trans. R. Soc., A* **2004**, *362*, 787.
[188] F. Huth, M. Schnell, J. Wittborn, N. Ocelic, R. Hillenbrand, *Nat. Mater.* **2011**, *10*, 352.
[189] a) T. Taubner, R. Hillenbrand, F. Keilmann, *Appl. Phys. Lett.* **2004**, *85*, 5064; b) J. M. Hoffmann, B. Hauer, T. Taubner, *Appl. Phys. Lett.* **2012**, *101*, 193105; c) F. Huth, A. Govyadinov, S. Amarie, W. Nuansing, F. Keilmann, R. Hilenbrand, *Nano Lett.* **2012**, *12*, 3973; d) M. Ishikawa, M. Katsura, S. Nakashima, Y. Ikemoto, H. Okamura, *Opt. Express* **2012**, *20*, 11064; e) J. S. T. Smalley, F. Vallini, S. A. Montoya, L. Ferrari, S. Shahin, C. T. Riley, B. Kanté, E. E. Fullerton, Z. Liu, Y. Fainman, *Nat. Commun.* **2017**, *8*, 13793.
[190] a) A. Centrone, *Annu. Rev. Anal. Chem.* **2015**, *8*, 101; b) E. Calandrini, T. Venanzi, F. Appugliese, M. Badioli, V. Giliberti, L. Baldassarre, P. Biagioni, F. De Angelis, W. M. Klesse, G. Scappucci, M. Ortolani, *Appl. Phys. Lett.* **2016**, *109*, 121104.
[191] a) F. Huth, A. Chuvilin, M. Schnell, I. Amenabar, R. Krutokhvostov, S. Lopatin, R. Hillenbrand, *Nano Lett.* **2013**, *13*, 1065; b) V. Giliberti, E. Sakat, M. Bollani, M. V. Altoe, M. Melli, A. Weber-Bargioni, L. Baldassarre, M. Celebrano, J. Frigerio, G. Isella, S. Cabrini, M. Ortolani, *Small Methods* **2017**, *1*, 1600033.
[192] P. Alonso-González, A. Y. Nikitin, F. Golmar, A. Centeno, A. Pesquera, S. Vélez, J. Chen, G. Navickaite, F. Koppens, A. Zurutuza, F. Casanova, L. E. Hueso, R. Hillenbrand, *Science* **2014**, *344*, 1369.
[193] a) S. Dai, Q. Ma, M. K. Liu, T. Andersen, Z. Fei, M. D. Goldflam, M. Wagner, K. Watanabe, T. Taniguchi, M. Thiemens, F. Keilmann, G. C. A. M. Janssen, S. E. Zhu, P. Jarillo Herrero, M. M. Fogler, D. N. Basov, *Nat. Nanotechnol.* **2015**, *10*, 682; b) Z. Fei, G. O. Andreev, W. Bao, L. M. Zhang, A. S. McLeod, C. Wang, M. K. Stewart, Z. Zhao, G. Dominguez, M. Thiemens, M. M. Fogler, M. J. Tauber, A. H. Castro-Neto, C. N. Lau, F. Keilmann, D. N. Basov, *Nano Lett.* **2011**, *11*, 4701.
[194] Z. Fei, J. J. Foley, W. Gannett, M. K. Liu, S. Dai, G. X. Ni, A. Zettl, M. M. Fogler, G. P. Wiederrecht, S. K. Gray, D. N. Basov, *Nano Lett.* **2016**, *16*, 7842.
[195] P. Li, T. Wang, H. Böckmann, T. Taubner, *Nano Lett.* **2014**, *14*, 4400.
[196] O. Khatib, J. D. Wood, A. S. McLeod, M. D. Goldflam, M. Wagner, G. L. Damhorst, J. C. Koepke, G. P. Doidge, A. Rangarajan, R. Bashir, E. Pop, J. W. Lyding, M. H. Thiemens, F. Keilmann, D. N. Basov, *ACS Nano* **2015**, *9*, 7968.
[197] E. Kauffmann, N. C. Darnton, R. H. Austin, C. Batt, K. Gerwert, *Proc. Natl. Acad. Sci. USA* **2001**, *98*, 6646.
[198] B. Schwarz, P. Reininger, D. Ristanic, H. Detz, A. M. Andrews, W. Schrenk, G. Strasser, *Nat. Commun.* **2014**, *5*, 4085.
[199] P. T. Lin, V. Singh, J. Wang, H. Lin, J. Hu, K. Richardson, J. D. Musgraves, I. Luzinov, J. Hensley, L. C. Kimerling, A. Agarwal, *Opt. Mater. Express* **2013**, *3*, 1474.
[200] M. J. Romeo, S. Boydston-White, C. Matthäus, M. Miljković, B. Bird, T. Chernenko, M. Diem, in *Biomedical Vibrational Spectroscopy*, John Wiley & Sons, Inc., Hoboken, NJ, USA **2007**, Ch. 6.
[201] A. T. Tokunaga, D. A. Simons, W. D. Vacca, *Publ. Astron. Soc. Pac.* **2002**, *114*, 180.
[202] J. M. Kahn, R. You, P. Djahani, A. G. Weisbin, T. Beh Kian, A. Tang, *IEEE Commun. Mag.* **1998**, *36*, 88.
[203] a) K. F. Lee, Y. Tian, H. Yang, K. Mustonen, A. Martinez, Q. Dai, E. I. Kauppinen, J. Malowicki, P. Kumar, Z. Sun, *Adv. Mater.* **2017**, *29*, 1605978; b) A. D. Greentree, B. A. Fairchild, F. M. Hossain, S. Prawer, *Mater. Today* **2008**, *11*, 22.
[204] Y. R. Shen, *The Principles of Nonlinear Optics*, John Wiley & Sons, Inc., NY **1984**.
[205] G. X. Ni, L. Wang, M. D. Goldflam, M. Wagner, Z. Fei, A. S. McLeod, M. K. Liu, F. Keilmann, B. Özyilmaz, A. H. Castro Neto, J. Hone, M. M. Fogler, D. N. Basov, *Nat. Photonics* **2016**, *10*, 244.